



The budgets of turbulence kinetic energy and heat in the urban roughness sublayer

Amir A. Aliabadi¹ · Mohsen Moradi¹ · Ryan A. E. Byerlay¹

Received: 2 October 2020 / Accepted: 8 June 2021 / Published online: 24 June 2021
© The Author(s), under exclusive licence to Springer Nature B.V. 2021

Abstract

Quantification of the terms in the transport equations of turbulence kinetic energy k and heat in the real urban roughness sublayer is inherently difficult due to variation of terms with thermal stability, wind speed, wind direction, and horizontal heterogeneity of most urban sites concerning morphometric parameters and land use. There is also a paucity of observations in the real urban environment, specifically pertaining to the heat budget, which motivate such budget analyses to understand the physical processes, inform urban development, and parametrize microclimate models. The budget terms of k and heat in the urban roughness sublayer were quantified using field observations conducted in the Reek Walk, Guelph, Canada, inside a quasi two-dimensional urban canyon located at the University of Guelph, from 15 July 2018 to 5 September 2018. The budget terms were analyzed under four stability classes, from thermally unstable to stable conditions, and under different wind speeds, from very low to high wind speed conditions. The budget terms were further analyzed under varying wind directions in eight sectors with respect to the canyon axis. For k , the budget terms quantified were storage, advection, buoyant production/consumption, shear production/consumption, turbulent transport, and dissipation. It was found that the main transport mechanism for k was driven by the turbulent transport that relocated k from the shear layer above roof (speculated but not measured) to the urban canyon, where it was balanced by shear production/consumption and dissipation terms. The advection term had lower magnitude to other terms but was greater in magnitude than the buoyant production/consumption term. For heat, the budget terms quantified were storage, advection, and flux divergence. It was found that the main transport mechanism for heat was driven by advection, where either warm or cold air masses were transported to the urban canyon depending on wind direction. The advection was found to be balanced by flux divergence. For both k and heat the storage terms were at least one order of magnitude smaller than other budget terms. For k it was found that with decreasing wind speeds, the residual (unexplained) portion of the budget increased, suggesting more difficulties in the Reynolds decomposition approach and budget apportionment in such cases. The findings for the k budget were in agreement with previous studies, while the findings for the heat budget could inspire further investigations. It was noted that the advective transfer mechanisms for heat could be overlooked in simplified urban microclimate models, but such transfer mechanisms need to be accounted for.

Extended author information available on the last page of the article

Keywords Budget · Heat · Turbulence · Turbulence kinetic energy · Urban canyon

1 Introduction

Airflow and temperature dynamics in the urban environment exhibit numerous complexities unlike typical atmospheric boundary layers observed in rural areas over flat and homogeneous lands. Specifically, the urban roughness sublayer (RSL), where individual roughness elements including buildings, trees, and vehicles influence the airflow and temperature dynamics, needs to be understood in greater detail [47]. One way to understand the complexities of the urban RSL is to conduct budget analysis of transport equations for momentum, heat, and turbulence kinetic energy k , where each term in the equations is experimentally or numerically approximated, hence quantifying the relative magnitude of transport mechanisms such as advection, flux divergence, diffusion, or various other source and sink terms. Below, first previous experimental attempts to perform budget analyses of the transport equations in flows with urban-like roughness elements are reviewed. Then research challenges are identified in these and other relevant investigations which warrant the need for alternative methodologies for budget analysis of transport equations. Finally, the objectives and the structure of the present paper are provided.

1.1 Budget analyses in the literature

Budget analyses of k for flows associated with urban-like or real urban elements have been conducted either at reduced scale [10, 11, 14, 49] or full scale [16, 32, 38]. Most studies describe a few persistent transport mechanisms for k . It has been found that at higher levels above roofs the shear or buoyancy production/consumption balance the dissipation rate, as expected in horizontally-homogeneous boundary layers [14, 16, 32]. Toward the surface, however, buoyancy or shear production/consumption reach a maximum level at roof level while turbulent transport relocates the produced k upward and downward away from this layer hence thickening the shear layer [10, 14, 16, 32, 49]. Dissipation rate reaches the maximum amount toward the canopy layer [32, 49]. It has been found that the layer within the canopy exhibits turbulent transport, pressure transport, and wake production/consumption from above, but negligible local production/consumption due to shear and buoyancy [16]. Studies have found that generally buoyancy production/consumption and storage terms are smaller in magnitude compared to other terms involving turbulent transport, shear production/consumption, and dissipation [38].

Budget analysis of heat for flows associated with real urban elements have been conducted at full scale [46]. Such investigations are much more limited compared to budget analysis of k . The only proposed transport mechanism within the canyon is the balance between flux divergence and heat storage [46]. Other transport mechanisms, such as advection, have not been studied.

1.2 Non-regularity of urban morphology

In the idealized urban morphologies, such as those found in regular two-dimensional canyons with cross-flow conditions, airflow modes are categorized in isolated roughness, wake interference, or skimming regimes, depending on the spacing of buildings relative to their characteristic lengths [42]. For convenience and the ability to generalize, many

observations of budget analysis or other flow properties are conducted over regular or staggered building arrays, either at partial scale [11, 14, 21, 23, 24, 49] or full scale [32]. However such idealization is seldom realized in real non-regular urban morphologies [58]. Real street canyons may be surrounded by tall or short buildings, parks, or other urban sites. Streets in many old cities are not positioned at right angles. Even in newer cities with right-angle street networks, building development is highly heterogeneous, involving the development of buildings with various heights. Such features create complex flow patterns involving down wash, wake, stagnation, edge-corner vortices, separation, reattachment, tunneling, and other effects. Further, complex heat exchange patterns may occur as a result of non-regular urban morphologies. In fact many studies carrying analysis in real urban fields noted the heterogeneity of the urban morphology, which implicated spatial variability or wind-direction variability of flow statistics [16, 25, 27, 28, 37, 38, 45, 46, 48, 59]. Although inconvenient, this necessitates more observations involving site-specific and non-regular building morphologies for budget analysis to apportion the terms of transport equations.

1.3 Field versus wind tunnel or scale model observations

Among the studies investigated, only four performed budget analysis at the full scale urban environment [16, 32, 38, 46], while others used wind tunnel or scale model observations. Reduced-scale observations suffer from few limitations because comprehensive scale-similarity with full scale observations cannot be achieved to ensure invariance of the Navier-Stokes equations with scale change. Even though geometric similarity may be achieved conveniently, aerodynamic and thermodynamic similarities are more difficult to achieve [24]. For aerodynamic similarity the earlier evidence suggested that reaching a building Reynolds number of $Re \sim 11,000$ is sufficient for a scale model, while recent observations provide evidence that a building Reynolds number as high as $Re \sim 87,000$ may be necessary, which is more difficult to achieve in a scale model [15]. Achieving thermodynamic similarity is even more problematic for scale models, since Richardson Ri or Grashof Gr numbers are seldom matched with a full scale observation [26]. This necessitates more observations at full scale for budget analysis to apportion the terms of transport equations.

1.4 Effects of thermal stability

For full scale observations, among the studies investigated for budget analysis and other flow properties, six considered various thermal stability levels [16, 27, 28, 38, 46, 59], while others only presented data records for near-neutral or thermally unstable conditions [25, 32, 36, 37, 45, 52, 55]. Klein and Clark [27] observed that under thermally stable conditions, the mean and turbulent transport mechanisms for momentum, k , and heat can change. Also the integral time and length scales as well as variances and fluxes of turbulence were observed to reduce under thermally stable condition [6]. Further, thermal stability impacts the flux-gradient relationships for momentum and heat [55, 59], apportionment of the terms of k equation [16], vertical profiles of mean and turbulence statistics for different variables [46, 55], and the turbulent Prandtl number [55]. This necessitates more observations at full scale for budget analysis to apportion the terms of transport equations considering thermally unstable, near neutral, and stable conditions.

1.5 Role of wind direction and speed

For full scale observations, and among the studies investigated for budget analysis, only three considered the impact of wind direction on the apportionment of the terms of transport equations [16, 38, 49]. Particularly in heterogeneous urban morphologies, mean building height, plan area density, and frontal area density may vary greatly according to the wind direction. Observations of Klein and Clark [27] and Klein and Galvez [28] showed great variability for components of wind speed and k as a function of wind direction for heterogeneous urban sites. Observations of Theeuwes et al. [55] also indicated variations in the profiles of wind speed and friction velocity as a function of wind direction. Also, budget analyses and the Reynolds decomposition approach become problematic when wind speed is too low, where record-to-record variability of terms in the transport equations are observed and the meteorological variables are subjected to low-frequency sub-mesoscale motions [52]. Such evidence calls for more rigorous analysis of the dependency of terms in the transport equations as a function of wind direction and speed (particularly low wind speed) for budget analysis.

1.6 Sparsity of heat budget investigations

From the reviewed literature, only one performed budget analysis to apportion the terms of the heat transport equation [46]. Even in that study, only the components of the flux divergence term were apportioned, while the components of the advection term were ignored. Observations of Theeuwes et al. [55] indicated that profiles of temperature, vertical turbulent sensible heat flux, and turbulent Prandtl number can vary greatly as a function of wind direction and thermal stability. Such limited evidence calls for more rigorous investigation of the dependency of terms in the transport equation for heat by budget analysis.

1.7 Horizontal components of terms in the transport equations

For full scale observations, and among the studies investigated for budget analysis, there was a lack of studies placing sensors at a horizontal distance to apportion the horizontal components of the terms in transport equations. Only two studies attempted horizontal placement of sensors nearby for budget analyses [38, 46] while others only relied on single-tower measurements [16, 32]. It must be noted that most real urban sites are highly heterogeneous, exhibiting spatial variation for most mean and turbulence statistics of the flow at the neighborhood scale and beyond [25, 59]. Even at the street canyon scale, horizontal variation of the mean and turbulence statistics of the flow variables can be expected given the fact that flows within the urban canopy can be understood as bluff body flows. For instance, placing two towers in the same street, Klein and Clark [27] found along-canyon and vertical variations in components of flow that persisted under various wind directions and created complex flow patterns in a street canyon, where the typical canyon vortex under idealized conditions could not be observed. Horizontal variations of the mean and turbulence statistics of the flow variables are important from the point of view of budget analysis to apportion the terms of the transport equations. For instance concerning the k equation, the advection, shear production/consumption, and turbulent transport terms are three directional and consist of terms in the cross-canyon, along-canyon, and vertical directions. Likewise in the heat equation, the advection and flux divergence terms are three directional and consist of terms in the cross-canyon, along-canyon, and vertical

directions. If only a single tower is used, the horizontal components of the terms in transport equations may either be ignored [32] or approximated by a surrogate method from a large ensemble of measured values under different conditions (e.g. wind direction) [16]. An alternative way is supported by placing limited number of sensors at a horizontal distance along and across a street canyon, forming a control volume, to quantify the horizontal components of the terms in the transport equations.

1.8 Objectives

From this review and identification of research challenges, it is imperative that more full scale observations should be conducted for budget analysis to understand the relative importance of the terms in transport equations of k and specifically heat inside a street canyon. The detailed questions to be answered are as follows. How can heterogeneity of a specific urban site with drastic change in land use and morphometric parameters affect the apportionment of the terms in the transport equation for k and heat? What are the effects of varying thermal stability, wind direction, and wind speed (particularly low wind speed) on the apportionment of the terms in the transport equations? How can the horizontal components of terms in the transport equations be approximated by placing sensors at a horizontal distance in the along-canyon and cross-canyon directions?

The current study aimed to apportion the budgets of k and heat inside a specific street canyon in a heterogeneous site with morphometric and land use variations along different directions. The budget terms in each of the k and heat equations were approximated using five ultrasonic anemometer measurements distributed along the three axes of the canyon coordinate system. For budget analysis, terms of the transport equations were analyzed either under four stability classes, from thermally unstable to stable conditions, or under different wind conditions from very low to high wind. In addition, the budget terms were further analyzed under varying wind directions in eight sectors with respect to the canyon axis. To explain, at depth, the physical processes influencing the apportionment of the terms in the heat transport equation, thermal imaging was conducted at the street-canyon and neighborhood scales to identify land surface temperatures.

In Sect. 2 we describe the transport equations for k and heat followed by the urban environmental monitoring site and instrumentation details. This section also provides the methodology for data processing, numerical approximation of the terms, and data classification. In Sect. 3 we provide the results and discussion. Sample numbers, background meteorological conditions, and error estimates are detailed in Sect. 3.1. Budget of k is discussed in Sect. 3.2. In Sect. 3.3 we provide results of thermal imaging analysis and land surface temperatures to further interpret the apportionment of the terms in the heat transport equation. Budget of heat is discussed in Sect. 3.4. In Sect. 4 we provide the conclusions and suggestions for future work.

2 Methodology

In this study Reynolds decomposition was used for analysis, i.e. $\Theta = \bar{\Theta} + \theta$, where Θ was the potential temperature (hereafter temperature), and $U_i = \bar{U}_i + u_i$, where $U_1 = U$, $U_2 = V$, and $U_3 = W$ were cross-canyon, along-canyon, and vertical components of wind velocity vector, respectively. Due to the lack of the availability of the ensemble average of a variable, i.e. $\langle U_i \rangle$, the half-hour time average of the variable, i.e. \bar{U}_i , was used instead.

2.1 Turbulence kinetic energy budget

Using Einstein's notation, turbulence kinetic energy can be expressed as $k = \frac{1}{2}\overline{u_i u_i}$. Note that k is by definition one half of the sum of the variances of wind velocity vector components, so use of over-bar on k should be avoided. The k equation is formulated as [53]

$$\underbrace{\frac{\partial k}{\partial t}}_S + \underbrace{\overline{U}_j \frac{\partial k}{\partial x_j}}_A = +\delta_{i3} \underbrace{\frac{g}{\Theta} (\overline{u_i \theta})}_{Pb} - \underbrace{\overline{u_i u_j} \frac{\partial \overline{U}_i}{\partial x_j}}_{Ps} - \underbrace{\frac{\partial (\overline{u_i u_i u_i})}{\partial x_j}}_{Tt} - \underbrace{\epsilon}_{D} - \underbrace{\frac{1}{\rho} \frac{\partial (\overline{u_i p})}{\partial x_i}}_{Pc}. \quad (1)$$

Term S is the local storage of k and is found to be negligible compared to other terms under quasi-statistically-stationary conditions, which is typical of half-hourly or hourly k budget analysis in the urban RSL [16, 38]. Nevertheless, it can be considered for our budget analysis. Term A is the advection of k that can be further decomposed into the sum of advection components from each of the three directions, i.e. $A = A_1 + A_2 + A_3$ or $A = A_x + A_y + A_z$. Note that if components of the advective term are apportioned, there is no need to apportion the budget terms due to dispersive transport. Rather, the dispersive transport phenomena are included in the advective terms [4]. Term Pb is the buoyant production/consumption of k that is non-zero only in the vertical direction. Here Θ is a reference temperature, in Kelvin, that can also be taken as the control volume average temperature. Term Ps is defined as shear production/consumption of k [53] that can further be decomposed into the sum of components from each of the three directions, i.e. $Ps = Ps_x + Ps_y + Ps_z$, with components given by

$$Ps_x = -\overline{u^2} \frac{\partial \overline{U}}{\partial x} - \overline{vu} \frac{\partial \overline{V}}{\partial x} - \overline{wu} \frac{\partial \overline{W}}{\partial x}, \quad (2)$$

$$Ps_y = -\overline{uv} \frac{\partial \overline{U}}{\partial y} - \overline{v^2} \frac{\partial \overline{V}}{\partial y} - \overline{wv} \frac{\partial \overline{W}}{\partial y}, \quad (3)$$

$$Ps_z = -\overline{uw} \frac{\partial \overline{U}}{\partial z} - \overline{vw} \frac{\partial \overline{V}}{\partial z} - \overline{w^2} \frac{\partial \overline{W}}{\partial z}. \quad (4)$$

Note that in simple boundary layers over flat terrain for flows with sufficient inertia, Ps_z usually exhibits an opposite sign to the mean vertical wind shear, because momentum flux is directed opposite to the gradient of the mean flow. Thus, the shear production/consumption term results in a positive contribution to k when multiplied by a negative sign. However, in complex geometries one cannot make this claim and assert that Ps (in any of the three directions) should always remain as a production term (i.e. make a positive contribution to k). In fact some components of Ps can be either positive or negative depending on the wind direction and placement of the sensors that quantify this term in complex three dimensional geometries such as in a street canyon. Term Tt is turbulent transport of k , describing how k is moved around by turbulent eddies. This term, also, can be decomposed into the sum of components from each of the three directions, i.e. $Tt = Tt_x + Tt_y + Tt_z$, with the components given by

$$Tt_x = -\frac{\partial \overline{uuuu}}{\partial x} - \frac{\partial \overline{uvvv}}{\partial x} - \frac{\partial \overline{uwww}}{\partial x}, \quad (5)$$

$$Tt_y = -\frac{\partial \bar{vuu}}{\partial y} - \frac{\partial \bar{vvv}}{\partial y} - \frac{\partial \bar{vwv}}{\partial y}, \quad (6)$$

$$Tt_z = -\frac{\partial \bar{wuu}}{\partial z} - \frac{\partial \bar{wvv}}{\partial z} - \frac{\partial \bar{wwv}}{\partial z}. \quad (7)$$

Term D is viscous dissipation of k , i.e. characterizing the conversion of k into heat. Term Pc is a pressure correlation term that describes how k is redistributed by pressure perturbations. It is often associated with oscillations in the air. Here $\bar{\rho}$ is the averaged density of air and p is pressure fluctuations. Of all the terms described above, the last term could not be directly quantified using field measurements in this work. This term, plus any other terms neglected and sources of error, can be grouped in a residual term R , i.e. $R = P_c + \text{Neglected Terms and Errors}$. With these considerations, the k budget equation can be written as

$$S = -A + Pb + Ps + Tt + D + R. \quad (8)$$

2.2 Heat budget

Heat conservation equation and Reynolds averaging result in the transport equation for temperature as [53]

$$\underbrace{\frac{\partial \bar{\Theta}}{\partial t}}_S + \underbrace{\bar{U}_j \frac{\partial \bar{\Theta}}{\partial x_j}}_A = \underbrace{+\nu_\theta \frac{\partial^2 \bar{\Theta}}{\partial x_j^2}}_{Mc} - \underbrace{\frac{1}{\bar{\rho} C_p} \frac{\partial \bar{Q}_j^*}{\partial x_j}}_{Rd} - \underbrace{\frac{L_v E}{\bar{\rho} C_p}}_{Lh} - \underbrace{\frac{\partial (\bar{u}_j \bar{\theta})}{\partial x_j}}_{Fd}. \quad (9)$$

Term S is the local mean storage of heat but cannot be necessarily considered as negligible in comparison to other terms in half-hourly or hourly heat budget analysis in the urban RSL due to paucity of heat budget analyses in the literature. Term A describes the advection of heat by mean wind that can be further decomposed into the sum of advection components from each of the three directions, i.e. $A = A_x + A_y + A_z$. Term Mc is mean molecular conduction of heat and can be assumed negligible in comparison to other terms due to advection and turbulent mechanisms transporting heat in the canyon scale. Term Rd is the mean net body source/sink term associated with radiation divergence. Term Lh is the body source/sink term associated with latent heat. Term Fd is the divergence of the turbulent heat flux that can be further decomposed into the sum of components from each of the three directions, i.e. $Fd = Fd_x + Fd_y + Fd_z$. Of all the terms discussed above, terms Rd and Lh could not be directly quantified using field measurements in this work. These terms, molecular conduction of heat Mc plus any other neglected terms and sources of error can be grouped in a residual term R , i.e. $R = Mc + Rd + Lh + \text{Neglected Terms and Errors}$. With these considerations, the heat budget equation can be written as

$$S = -A + Fd + R. \quad (10)$$

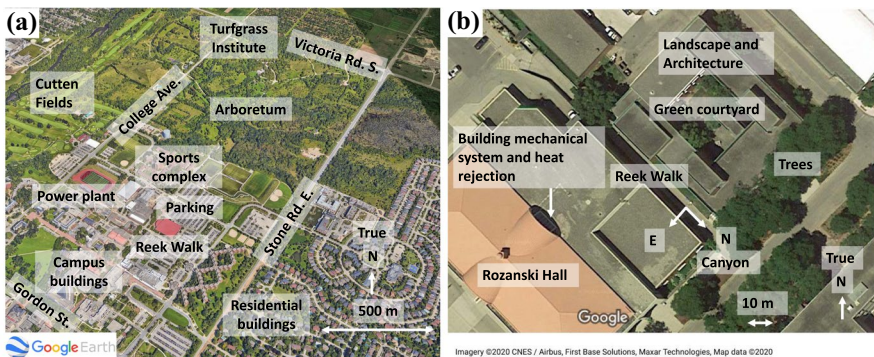


Fig. 1 View of the urban area for the microclimate field campaign in Guelph, Canada; **a** neighborhood view of the Reek Walk, where urban measurements were conducted, and the surrounding areas; **b** canyon view of the Reek Walk adjacent to the Rozanski Hall on the east of the street canyon and the Landscape and Architecture building on the west of the street canyon

Table 1 Classification of morphometric parameters as a function of wind direction in eight sectors with respect to the canyon axis north direction. The parameters are determined considering a radius of 200 m around the urban measurement site

	N	NE	E	SE	S	SW	W	NW	Average
\bar{H} [m]	17	14	14	20	7	7	13	14	13.25
λ_p [-]	0.61	0.32	0.20	0.33	0.24	0.47	0.60	0.36	0.39
λ_f [-]	0.16	0.18	0.10	0.23	0.04	0.09	0.11	0.15	0.13

2.3 Urban environmental monitoring site

The urban microclimate field campaign was conducted from 15 July 2018 to 5 September 2018 in Guelph, Canada. Guelph is situated in south-western Ontario, Canada, characterized by cold winters and humid summers. The measurements were conducted in the Reek Walk, a typical quasi two-dimensional urban canyon, located at the University of Guelph (43.5323°N and 80.2253°W). Figure 1 shows the view of the urban area for the microclimate field campaign, featuring the measurement locations and the surrounding environment.

Table 1 shows the classification of morphometric parameters including average building height \bar{H} , plan area density λ_p , and frontal area density λ_f associated with wind direction in eight sectors with respect to the canyon axis north (λ_p and λ_f defined by Oke et al. [43]). These parameters are calculated using buildings identified in Google Earth within a radius of 200 m around the urban measurement site. According to this table the urban site is highly heterogeneous since morphometric parameters change according to the wind sector. The average building height of the urban area is $\bar{H} = 13.25$ m. The average plan and frontal area densities are $\lambda_p = 0.39$ and $\lambda_f = 0.13$, respectively.

Figure 2 shows the location for the urban measurements and the control volume considered for budget analysis of k and heat in detail. The road, Reek Walk, where meteorological instruments were installed, is covered by grass and asphalt in equal fractions. The building height and width for the urban canyon, in which measurements took place, are $H = 13$ m

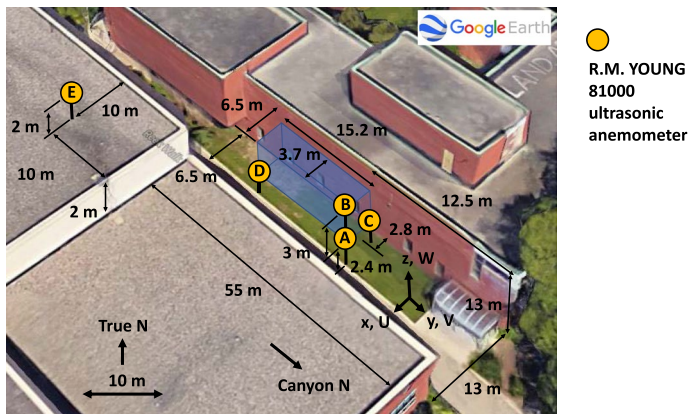


Fig. 2 View of the locations for the urban measurements and the control volume considered for budget analyses of k and heat

and $W = 13$ m, respectively. The urban canyon axis is oriented north-west-south-east. The x and y coordinate directions are cross- and along-canyon, respectively. Given the wind direction, the wind flow pattern classification in the canyon should have alternated between skimming flow and wake interference regimes [19, 58]. However, the actual wind flow pattern could be more complicated given the heterogeneity of the urban environment.

2.4 Instrumentation

The list of instrumentation is provided in Table 2. In the urban site, meteorological information was collected within and above the canyon using five ultrasonic anemometers (81000, R. M. Young Company, Traverse City, Michigan, USA) distributed horizontally and vertically. The accuracy and resolution of measurements for wind speed were $\pm 1\%$ and 0.01 m s^{-1} , respectively, and for temperature were $\pm 2 \text{ K}$ and 0.01 K , respectively. In the canyon coordinate system, the x , y , and z axes were cross-canyon, along-canyon, and vertical directions, respectively. As shown in Fig. 2, four anemometers (A-D) were deployed within the canyon to form a rectangular box-shaped control volume aligned with the street canyon. Anemometers A, C, and D were deployed at a height of 2.4 m from ground while anemometer B was deployed at 5.4 m above ground.

Table 2 Instrumentation used in the field monitoring campaigns; locations are specified in Fig. 2; the temperature calibration for all ultrasonic anemometers were conducted in the same location (A) before each anemometer was placed in its designated location; the ground-based thermal camera (E4) took images from location (A); the airborne thermal camera (Zenmuse XT) was launched from location (A)

Instrument	Model (Manufacturer)	Location	Measurements
Ultrasonic anemometers	81000 (R.M. Young)	A-E	Wind, air temperature
Dataloggers	CR6 (Campbell Scientific)	A-E	Wind, air temperature
Temperature sensor	HMP60 (Vaisala)	A	Air temperature
Thermal camera	E4 (FLIR)	A	Surface temperature
Thermal camera	Zenmuse XT (FLIR)	A	Surface temperature

Anemometers A, B, and D were at the central axis of the canyon, 6.5 m away from the south-west and north-east walls. Anemometer C was situated 2.8 m from the north-east wall. The control volume dimensions were $3.7\text{ m} \times 3\text{ m} \times 15.2\text{ m}$ and the control volume side was at a distance of 12.5 m away from the street intersection. The roof anemometer E was positioned at a height of 17 m above ground (2 m above roof level) and it was 10 m away in both x and y directions from the corner of a nearby roof. The positioning was arranged so each anemometer was at least 2 m away from any surface to avoid measuring any wall effects. The control volume box was elongated along-canyon since previous evidence suggested that the turbulent structures exhibited greater integral length and time scales along-canyon in comparison to cross-canyon and vertical directions [6]. For turbulence studies, it has been suggested to sample micro meteorological variables at a frequency greater than 10 Hz [2, 7, 18]. The anemometers were set to sample data at 20 Hz using data loggers (CR6, Campbell Scientific, Logan, Utah, USA). Throughout the campaign, the anemometers were frequently adjusted using a level device and oriented along the canyon axis using a compass to ensure they remained horizontal and measured the correct components of wind velocity vector. Ideally, more ultrasonic anemometers could have been deployed on a flux tower, covering multiple elevations below and above the canyon height, to observe the shear layer above the canyon; however, having access to only five ultrasonic anemometers, in this study the measurements were focused on inside the canyon.

Wind tunnel tests were conducted to calibrate the wind velocity components measured by the ultrasonic anemometers against a reference pitot tube. In an extended outdoor experiment, a temperature sensor (HMP60, Vaisala, Helsinki, Finland) was used as the reference temperature to calibrate all other temperatures measured by the ultrasonic anemometers [35]. This sensor measured the temperature with an accuracy of $\pm 0.6\text{ K}$, with a sampling frequency of 10 min during the calibration.

Thermal imaging was conducted at the street canyon and neighborhood scales to quantify surface temperatures to assist understanding of the physical processes related to budget analysis of the terms in the heat transport equation. At the street canyon scale, thermal imaging of the urban surfaces was performed using a thermal camera (E4, FLIR, Wilsonville, Oregon, USA) in a campaign that was conducted in the previous year from 13 to 25 August 2017 [6]. During intensive observation periods on 14 and 23 August 2017, this camera was pointed at multiple locations including the roof (one location), canyon walls (six locations), asphalt (two locations), and grass (two locations). During these periods three measurements at each location were made at 1-h time intervals. Images collected were processed statistically by calculating mean temperatures and the standard deviations at every location for every hour. More than 1,500 thermal images were analyzed (see Aliabadi et al. [6] for more details). These two days corresponded to conditions representative of clear skies with moderate wind speeds.

At the neighborhood scale, thermal imaging of the urban surfaces was performed using a thermal camera (FLIR Zenmuse XT Radiometric, Wilsonville, Oregon, USA) on-board of a Tethered Air Blimp (TAB) [13, 35]. This system mapped earth surface temperatures with an accuracy of 0.5 K. It was launched every hour (except for 0000 to 0400 Local Standard Time (LST = UTC - 5)) on 28 July 2018 and 13 August 2018 to collect more than 7,000 images. The images were processed and their pixels were georeferenced (using the camera's altitude, latitude, longitude, tilt, and yaw angles) to provide surface temperatures at a horizontal resolution of $50\text{ m} \times 50\text{ m}$. This method allowed collecting numerous measurements in tiles of this resolution and calculating the four-hourly mean temperature in each tile (see Byerlay et al. [13] for more details).

2.5 Data analysis and quantification of terms in the budget equations

Figure 3 outlines the steps taken in the workflow demonstrating the record preparation, calculation of terms in the budget equations, and classification of data. Letters A-E in this figure correspond to anemometers shown in Fig. 2. Sections 2.5.1 to 2.5.3 provide detailed explanations for each step of the workflow and a process to estimate errors in measuring each of the budget terms.

2.5.1 Data processing and numerical approximations to calculate the budget terms

Various periods of averaging have been used in the literature for micro meteorological turbulence studies ranging from 15 min [7], to 30 min [6, 8, 9, 28] and 1 hr [8, 16]. Throughout the analysis, half-hour averaging was used to calculate the flow mean and turbulence statistics variables [20]. The averaging time ensured enough number of records were collected for statistical analysis. Also, compared to 1-hr averaging, 30-min averaging was expected to reveal micro meteorological processes with a lower influence from meso scale meteorological processes. Records associated with rain condition or traffic in the street canyon were eliminated. The friction velocity of the flow $u_* = (\overline{uw}^2 + \overline{vw}^2)^{1/4}$ was determined using the roof level anemometer (anemometer E in Fig. 2). Data was discarded if $u_* < 0.1 \text{ m s}^{-1}$ given the difficulty to determine wind direction and wind velocity vector components accurately at low velocities [16, 20]. While calculating turbulence statistics, many previous studies linearly detrended the variable signals [6, 23, 52], however we did not detrend the variable signals to ensure no amount of energy was removed so that the energy conservation was not violated [16].

To determine the time derivatives, i.e. storage terms, first a second order polynomial was fitted to three consecutive half-hour measurements of k or Θ , and then the slope of the fitted polynomial at the mid point was taken. Calculation of the budget terms require either

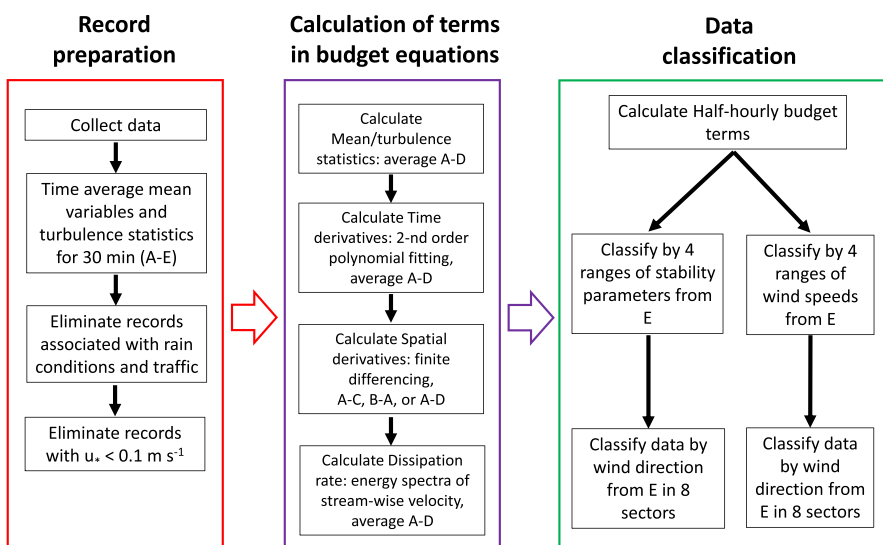


Fig. 3 Workflow demonstrating the record preparation, calculation of terms in the budget equations, and classification of data; letters A–E refer to anemometers identified in Fig. 2

mean or turbulence statistics (e.g. $\overline{u_i u_j}$ in the shear production/consumption term $P_s = -\overline{u_i u_j} \frac{\partial \bar{U}_i}{\partial x_j}$) or spatial derivatives of mean or turbulence statistics (e.g. $\frac{\partial \bar{U}_i}{\partial x_j}$ in the shear production/consumption term $P_s = -\overline{u_i u_j} \frac{\partial \bar{U}_i}{\partial x_j}$). The mean or turbulence statistics in the transport equations were calculated by averaging the measurements every half hour using anemometers A, B, C, and D (Fig. 2). This approach was justified given the spatial variability of flow in the urban canyon, where spatial averaging provided more representative quantities throughout the control volume. However, spatial derivatives were computed with respect to the canyon coordinate system shown in Fig. 2. In our case, since only two measurement locations were available to determine the spatial derivatives in each direction, we used simple finite differencing, where derivatives in the x direction were calculated using anemometers A and C (A-C), derivatives in the y direction were calculated using anemometers A and D (A-D), and derivatives in the z direction were calculated using anemometers A and B (B-A), according to Fig. 2. To determine the spatial derivatives, various methodologies have been used in the literature. When analyzing the vertical profiles of wind speed in the surface layer, Nieuwstadt [39] suggested using a logarithmic plus linear law, while Högström [20] suggested a second-order polynomial to calculate the vertical wind speed gradient using at least three measurement points. These methods were close to each other while estimating the vertical gradient of wind speed [59]. Christen et al. [16] approximated the vertical gradient of wind velocity by the local derivative of a parametric cubic spline interpolation with the lower boundary set to zero at the ground and a relaxed upper boundary at the topmost measurement level. While these methods apply to determining the vertical gradients, only the second-order polynomial method can be applied to determine the horizontal gradients [38]. Use of finite differencing in determination of spatial derivatives were reported by Ramamurthy et al. [46]. Numerical errors associated with this methodology would be absorbed in the residual term for each transport equation.

The spectral energy density of horizontal stream-wise wind velocity have been typically used to calculate the dissipation rate in the inertial subrange of the energy cascade [10, 14, 16, 38]

$$\epsilon = \left(\frac{1}{C} E_U(\kappa) \kappa^{\frac{5}{3}} \right)^{\frac{3}{2}}, \quad (11)$$

where ϵ is the dissipation rate, κ is the wave number, and $E_U(\kappa)$ is the spectral energy density function for the along-wind component of wind velocity vector. Here C is a constant taken to be close to 0.53 [10, 38, 52]. Here the stream-wise component of velocity is typically chosen since it has the longest sampled inertial subrange, providing a more accurate estimate of the dissipation rate [31, 52]. In this study the wave number was estimated using the Taylor's hypothesis [54] by $\kappa = 2\pi n/(P\bar{U})$, where n was the number of cycles in the time period of analysis, $P = 30$ min was the period of analysis, and \bar{U} was the time-averaged horizontal velocity component of the flow at each half-hour interval [5]. The dissipation rate was calculated considering the average of calculations from anemometers A-D in Fig. 2, which defined the control volume. Before calculating the spectral energy density, the coordinate reference frame was rotated around the z axis such that a new x axis was aligned with the half-hour-averaged wind direction [16]. To specify the wave number at which the dissipation rate is evaluated, a wave number should be used where $E_W(\kappa)/E_U(\kappa)$ reaches a value of 4/3 [16, 38, 49], and the wave number should fall within the inertial subrange with a slope of $-5/3$ for the energy spectrum versus the wave number in logarithmic scale [22, 52]. The sampling frequency of 20 Hz deemed sufficient for identification

of the inertial subrange of turbulence for determination of the dissipation rate. The same sampling frequency was used by Christen et al. [16] using the same method of determining the dissipation rate. Of course the use of Taylor's hypothesis for flows inside urban canyons has limitations, but this assumption is typically used for lack of a better assumption [6, 16, 36, 37, 44].

Figure 4 shows the spectral energy density function for the along-wind component normalized by the along-wind variance as well as the ratio of the vertical to along-wind components of the spectral energy density functions. These spectra are associated with the quality-controlled records throughout the campaign. The slope of $-5/3$ associated with the inertial subrange is observed for all anemometers over two orders of magnitude for the wave number. However, the theoretical value of $4/3$ for the ratio of spectra is only observed for the roof anemometer E while the lowest ratio is observed for anemometer C closest to the canyon wall. This is in agreement with observations of Christen et al. [16] who also reported a lower ratio for measurements inside an urban canyon (see their Fig. 6). The dissipation rate inside the canyon is estimated using the wave number for which ratio of spectra is maximized.

2.5.2 Error estimation for budget terms

Various errors can be identified in quantification of the budget terms. Such errors arise from accuracy of anemometers, finite temporal averaging, and estimation of spatial derivatives by finite differencing using anemometers A-D. The instruments were calibrated for their accuracy of measuring wind velocity components and air temperature, and the calibration curves were used to correct the data, so we exclude errors due to instrument accuracy from this section.

Due to finite temporal averaging, it is expected to encounter random and systematic errors in the measurement of turbulence statistics such as second (e.g. $\overline{u^2}$ and \overline{uv}) or third order (e.g. \overline{uuu}) moments and fluxes [3, 30]. Random errors can result in both overestimation or underestimation of the turbulence statistics, and they reduce by a factor of $1/\sqrt{N}$, when turbulence statistics are averaged over N records [3]. On the other hand, systematic errors always result in underestimation of the magnitude of the turbulence statistics, and

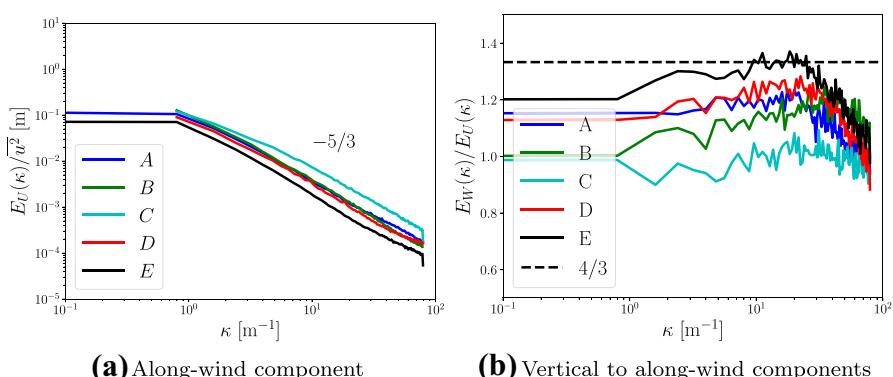


Fig. 4 **a** Spectral energy density function for the along-wind component normalized by the along-wind variance; **b** ratio of vertical to along-wind components of the spectral energy density functions; letters A-E refer to anemometers identified in Fig. 2

they do not reduce when averaged over multiple records [3]. The random relative errors associated with second and third order turbulence statistics can be computed as $\sqrt{\frac{2}{N}\frac{\tau}{T}}$ and $\sqrt{\frac{4}{N}\frac{\tau}{T}}$, respectively, subject to $T \gg \tau$, where τ is the integral timescale associated with the statistics being measured and T is the length of the record [3, 30]. Each integral time scale can be calculated by integrating the normalized autocorrelation function $\rho(s)$ associated with the turbulence statistic from a time shift of $s = 0$ to a time shift s^* , where the first zero crossing of the function occurs, i.e. $\tau = \int_{s=0}^{s^*} \rho(s)ds$ [1]. More details about the computation of τ and $\rho(s)$ can be found [2, 3, 30]. The systematic relative error associated with second and third order turbulence statistics can be computed as $2\frac{\tau}{T}$ and $5\frac{\tau}{T}$, respectively, subject to the same conditions. These errors can be computed and reported separately for each budget term using the theory of error propagation.

Estimation of the errors due to finite differencing to compute the spatial derivatives is more difficult. The most common technique to measure spatial derivatives is to deploy many sensors (≥ 3) along a coordinate direction (x , y , or z) and fit a polynomial, logarithmic, or spline curve through the measurements. The gradient can then be found by differentiating the curve at a desired point [16, 20, 38, 39, 59]. Once this gradient is known, the error associated with estimating the spatial derivative by finite differencing can be computed. In the present work only two anemometers were spanned in any given direction, so fitting of higher order curves to determine the gradient was not possible, nor was it possible to precisely quantify the error associated with estimating the spatial derivatives by finite differencing. In an experimental setup similar to the present work, Nelson et al. [38] reported relative errors due to finite differencing to be in the order of 0.1 in estimating spatial derivatives. In the present analysis we assume a fixed relative error of 0.1 due to finite differencing in the estimation of the spatial derivatives. This error can be computed and reported separately for each budget term using the theory of error propagation.

2.5.3 Data classification

Data classification was performed according to thermal stability, wind speed, and wind direction measured by the roof anemometer (E). For each classification, a further sub-classification was made according to wind direction. Two choices were available for thermal stability classification: 1) the stability parameters and 2) the bulk Richardson number. The thermal stability parameter $\zeta = (z - z_d)/L$ was determined using the roof level anemometer. Here $z = 17$ m was the height of the anemometer from the canyon floor, while $z_d = 0.7\bar{H}$ was a rough estimate of the displacement height [19]. The Obukhov length was $L = -\bar{\Theta}u_*^3/(\kappa gw\theta)$, where $\bar{\Theta}$ was the half-hourly-averaged temperature, $\kappa = 0.41$ was the von Kármán constant, $g = 9.81$ m s⁻² was the gravitational acceleration, and $w\theta$ was the vertical component of kinematic turbulent sensible heat flux, all measured by anemometer E. This provided the local Obukhov length (and not the Obukhov length for the surface layer, which must be computed at the bottom of the inertial sublayer, or equivalently the top of the urban RSL). Ideally Obukhov length should be computed at an elevation where $z/\bar{H} > 2$, however the present study is limited in this regard. The choice of thermal stability parameter using Monin–Obukhov similarity theory above roof level has been justified in literature by the fact that above roof level turbulence is typically mainly dependent on shear and buoyancy production/consumption [16]. The other choice of classification for thermal stability was the bulk Richardson number Ri_b calculated between street level and roof level [6], where typically a critical bulk Richardson number is used to define the stable versus unstable condition [41]. However, for consistency with other budget analyses

in the literature we used the thermal stability parameter. Data was discarded if $\zeta < -10$ or $\zeta > +10$ based on the justification that such thermal stability conditions are rare and that those conditions do not provide enough samples for statistical analysis. Four data groups were considered: *unstable* ($-10 < \zeta < -0.5$), *weakly unstable* ($-0.5 < \zeta < -0.1$), *near neutral* ($-0.1 < \zeta < +0.1$), and *stable* ($+0.1 < \zeta < +10$). The cut-off values of $\zeta = \pm 0.1$ and ± 0.5 are typically used in urban RSL studies to classify thermal stability levels and group data with a large enough statistical sample in each group [16, 55].

For classification of data based on wind speed, thresholds for wind speed should be defined. One of the problems in budget analysis and the Reynolds decomposition approach occurs when the wind speed is too low. As wind speeds decrease, large record-to-record variability occurs for urban climate variables, and the variables become subjected to low-frequency sub mesoscale motions [52]. Therefore, of particular interest was to classify the data to include such conditions. Low wind speed conditions are typically identified by calculating the statistic σ_H/WS where $\sigma_H = \sqrt{u^2 + v^2}$ is the horizontal velocity standard deviation and $WS = \sqrt{U^2 + V^2}$ is the mean horizontal wind speed. This quantity is related to the relative strength of the sub mesoscale motions compared to that of the mean flow. Low wind conditions occur when this quantity is at least twice as that under high wind condition [52]. For a suburban area with similar morphometric variables to this study the threshold wind speed for low wind conditions was calculated as 1 m s^{-1} [52, 57]. In our study the threshold wind speed for low wind conditions was also calculated as 1 m s^{-1} based on the roof anemometer (E). This formed the basis of defining the following thresholds in this study based on the roof anemometer (E) wind speed measurement: *very low wind* ($WS < 0.5 \text{ m s}^{-1}$), *low wind* ($0.5 < WS < 1 \text{ m s}^{-1}$), *moderate wind* ($1 < WS < 1.5 \text{ m s}^{-1}$), and *high wind* ($WS > 1.5 \text{ m s}^{-1}$). These ranges also ensured there was a large enough statistical sample in each group. Such classification of data based on wind speed was also used by Trini-Castelli et al. [57] and Schiavon et al. [52].

For each type of classification, data was further sub classified based on the wind angle at roof level α with respect to the canyon axis. In this sub classification the canyon north was along the $+y$ direction and eight 45-degree sectors were considered: *north* ($\alpha > 337.5^\circ$ and $\alpha < 22.5^\circ$), *north-east* ($22.5^\circ < \alpha < 67.5^\circ$), *east* ($67.5^\circ < \alpha < 112.5^\circ$), *south-east* ($112.5^\circ < \alpha < 157.5^\circ$), *south* ($157.5^\circ < \alpha < 202.5^\circ$), *south-west* ($202.5^\circ < \alpha < 247.5^\circ$), *west* ($247.5^\circ < \alpha < 292.5^\circ$), and *north-west* ($292.5^\circ < \alpha < 337.5^\circ$). As shown in Fig. 1 and Table 1, in each sector the morphometric parameters, building types, vegetation cover, and land use change, hence justifying the sub classification. The number of sub classifications and the ranges defined were also selected in a way to provide enough samples in each set for statistical analysis.

3 Results and discussion

3.1 Background meteorological conditions, number of samples, and error estimates

To understand the background meteorological conditions in connection with the thermal stability and wind speed classifications, it is first necessary to study diurnal variation of wind speeds and wind direction as measured by the roof anemometer E. Figure 5 shows

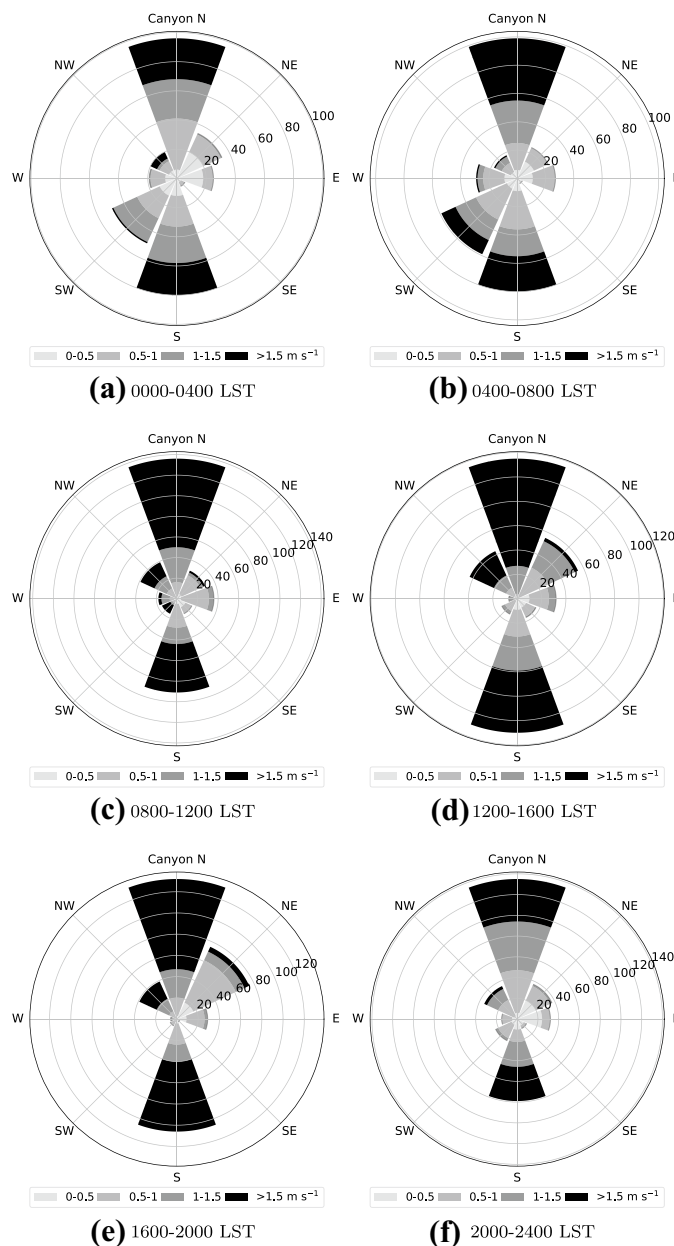


Fig. 5 Wind rose plot showing frequency of wind speed and direction observations with respect to the canyon north axis, as measured by the roof anemometer E, specified as the +y axis in Fig. 1, over the duration of the campaign; wind frequency plots were classified in four-hourly time windows; **a** 0000-0400 LST; **b** 0400-0800 LST; **c** 0800-1200 LST; **d** 1200-1600 LST; **e** 1600-2000 LST; **f** 2000-2400 LST; times in Local Standard Time (LST = UTC - 5)

the wind rose plot specifying the frequency of wind speed and direction with respect to the canyon north axis, specified as the $+y$ axis in Fig. 1, over the duration of the campaign. Wind frequency plots were classified in four-hourly time windows. There was a higher frequency of wind directions along the canyon axis, i.e. from canyon north or south, while there was a lower frequency of wind directions across the canyon (east or west) or at oblique angles (north-east, south-east, south-west, and north-west). Beside the north-south axis, it was noted that wind direction from other sectors could be asymmetric. For instance during thermally stable conditions in the early morning (0000–0400 and 0400–0800 Local Standard Time (LST = UTC - 5)), a higher frequency of wind directions were noted from south-west in comparison to north-east. The implications of such patterns in wind direction on the budget terms will be discussed later.

Table 3 shows the number of samples collected under different thermal stability and wind speed conditions. The table further breaks down the number of samples associated with each wind direction, with respect to the canyon north. The classification ranges are fully specified in Sect. 2.5.3. Each sample was collected for 30 min, and in total, 2119 samples (1059.5 hr of data) were processed for the budget analyses. It can be seen that the lowest number of samples were associated with south-east and west wind directions, where 55 and 87 samples were collected, respectively. The table shows that for most thermal stability, wind speed, and wind direction conditions, at least ten samples were identified, with the exception of seven cases out of 64 in the entire table, where less than ten samples were collected. Budget analyses for these cases should be performed with care. In

Table 3 Number of samples, each collected for 30 min, under different thermal stability and wind speed conditions; number of samples further shown under different wind directions, with respect to the canyon north, for each thermal stability or wind speed condition; classification ranges specified in Sect. 2.5.3

	Unstable	Weakly unstable	Near neutral	Stable	Total
North	66	170	348	106	690
North-east	10	73	132	34	249
East	7	51	88	30	176
South-east	8	22	16	9	55
South	38	164	268	60	530
South-west	10	13	85	41	149
West	10	29	32	16	87
North-west	57	49	61	16	183
Total	206	571	1030	312	2119
	Very low wind	Low wind	Moderate wind	High wind	Total
North	15	121	183	371	690
North-east	72	128	39	10	249
East	72	90	14	0	176
South-east	32	22	1	0	55
South	43	118	126	243	530
South-west	23	65	40	21	149
West	22	43	18	4	87
North-west	12	52	55	64	183
Total	291	639	476	713	2119

the subsequent analyses, all wind directions are reported with respect to the canyon north, unless otherwise stated.

Table 4 shows estimates of median random and systematic errors due to finite temporal averaging as well as the error associated with finite differencing to calculate spatial derivatives. Random errors are computed assuming an average sample size of $N = 66$, i.e. 2119 records divided by 32 sub classifications. For most budget terms, except for the residual term, random errors are typically lower than 10 %, while systematic errors could be higher. Errors due to finite differencing for the calculation of spatial derivatives are on average about 10 %. Systematic errors for the k budget terms can reach up to 41 % for determination of turbulent transport terms due to their dependency on third order turbulence statistics, which exhibit larger integral time scales compared to other turbulence statistics. The systematic errors for the turbulent transport terms are the main contributor to the residual term. This indicates that in fact the turbulent transport terms should contribute a greater amount toward the budget since systematic errors always result in underestimation of the magnitude of the turbulence statistics. Systematic errors for the heat budget terms can reach up to 17 % for the flux divergence terms, particularly for the along-canyon direction. This is due to the long integral time scale for the turbulent flux of heat in the along-canyon direction. Given the limitations of this study, the combined effect of the three types of errors cannot be estimated reliably, but in the subsequent analysis we expect the percent contribution of the residual terms to the overall budget be in the same order of magnitude as the computed errors for the residual term.

3.2 Turbulence kinetic energy budget

3.2.1 Diurnal variation

Although the day-to-day diurnal variability of stability parameter, wind speed, and wind direction could be significant, it is informative to study the diurnal variation of the terms in the k equation before the budget analysis of the terms classified per stability parameter, wind speed, and wind direction. Figure 6 shows the medians of the budget terms as they varied diurnally. These statistics were calculated based on all observations at the same hour.

The storage term S was two orders of magnitude smaller than other terms in agreement with previous findings [38], so it could be assumed that k met the quasi-statistically-stationary condition. This assumption has also been common in previous studies of the k budget [10, 12, 14, 16, 32, 56]. The negative of advection term $-A$ had the tendency to be positive making a contribution in increasing k , indicative of the fact the k could be transported from locations with higher intensities of k than the canyon. Although not directly measured, it is speculated that the shear layer above roof height was a major contributor for advection of k into the canyon. Although less in magnitude compared to other budget terms (P_s , T_t , and D), the advection mechanism of transport for k was only reported by Blackman et al. [10]. The buoyant production/consumption term P_b , too, was lower in magnitude compared to other budget terms ($-A$, P_s , T_t , and D), but it had the tendency to be positive at most diurnal times. This behaviour has been justified by the fact that, under certain circumstances, urban surfaces could be at higher temperatures compared to the air above surface even at nights, resulting in a positive P_b at nighttime too [38]. The other budget terms exhibited higher magnitudes than S , $-A$, and P_b , and indicated a balance between shear production/consumption P_s , turbulent transport T_t , and dissipation D . During daytime, it

Table 4 Median random (E_r) and systematic (E_s) errors in budget terms due to finite temporal averaging; errors in budget terms due to finite differencing for calculation of spatial derivatives (E_f); methodology described in Sect. 2.5.2

k	S	$-A_x$	$-A_y$	$-A_z$	$-A$	Pb	P_{S_x}	P_{S_y}	P_{S_z}	Ps	T_x	T_y	T_z	Tt	D	R
E_r [%]	2.5	3.6	3.6	3.6	6.0	1.2	2.2	2.1	1.0	2.7	8.4	9.6	6.6	11	5.7	12
E_s [%]	3.6	5.1	5.1	5.1	9.6	1.2	3.6	3.2	1.2	5.2	33	41	21	47	7.2	37
E_f [%]	-	10	10	10	16	-	12	9.9	8.1	13	12	9.5	7.1	11	-	9.8
Heat	S	$-A_x$	$-A_y$	$-A_z$	$-A$	Fd_x	Fd_y	Fd_z	Fd	R						
E_r [%]	-	-	-	-	-	-	-	-	-	-	4.5	6.0	2.3	7.1	1.2	
E_s [%]	-	-	-	-	-	-	-	-	-	-	10	17	2.5	25	3.8	
E_f [%]	-	10	10	10	10	11	10	10	10	10	10	10	13	11		

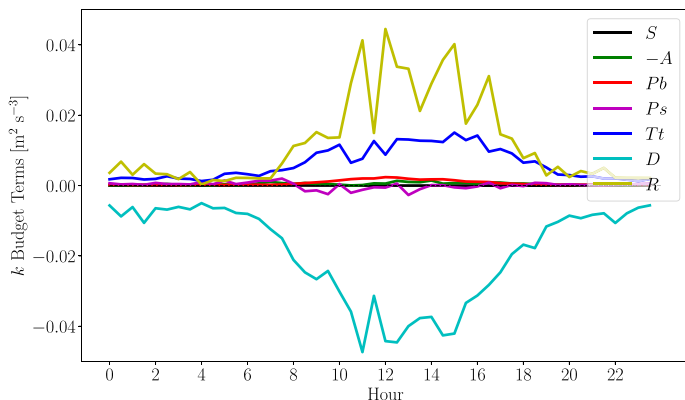


Fig. 6 Diurnal variation of terms in the budget of k ; budget apportioned according to terms described in Eq. 8; the medians are shown for every half-hour period; times are in Local Standard Time (LST = UTC - 5)

appeared that Tt (positive) transported k into the control volume from locations with higher intensities of k , possibly above the control volume and elsewhere, while it was balanced by Ps and D . This behaviour has been commonly reported in previous studies [10, 12, 14, 16, 17, 32, 49]. As evidence was provided in Table 4, the main contributor to the residual term is the turbulent transport term, for which the magnitude is underestimated due to the large systematic error.

3.2.2 Variation by thermal stability

Figure 7 and Table 5 show the apportionment of the budget of k according to different thermal stability parameters and wind directions. The relevant statistic in this case was the median of each term of Eq. 8 for a combination of thermal stability parameter and wind direction with ranges specified in Sect. 2.5.3. The budget contributions [% C], for either the total budget or the budget associated with directional terms, are presented as the percent contribution of the median of each term to the summation of the magnitude of the median of all terms, i.e.

$$\%C = \frac{100 \times \text{Budget term}}{|S| + |-A| + |Pb| + |Ps| + |Tt| + |D| + |R|}, \quad (12)$$

$$\%C = \frac{100 \times \text{Budget term}}{|-A_x| + |-A_y| + |-A_z| + |Ps_x| + |Ps_y| + |Ps_z| + |Tt_x| + |Tt_y| + |Tt_z|}, \quad (13)$$

respectively. Note that with this definition, ignoring the sign of the contribution of each term, the percent magnitude contribution of all budget terms should exactly add up to 100 % for each combination of thermal stability parameter and wind direction.

In the figure, first, in panels (a), (b), (c), and (d) the budget terms in Eq. 8 were quantified and visually demonstrated based on different ranges of thermal stability parameter and wind direction. Next, in panels (e), (f), (g), and (h), the directional components of the budget were broken down along the x (cross-canyon), y (along-canyon), and z (vertical)

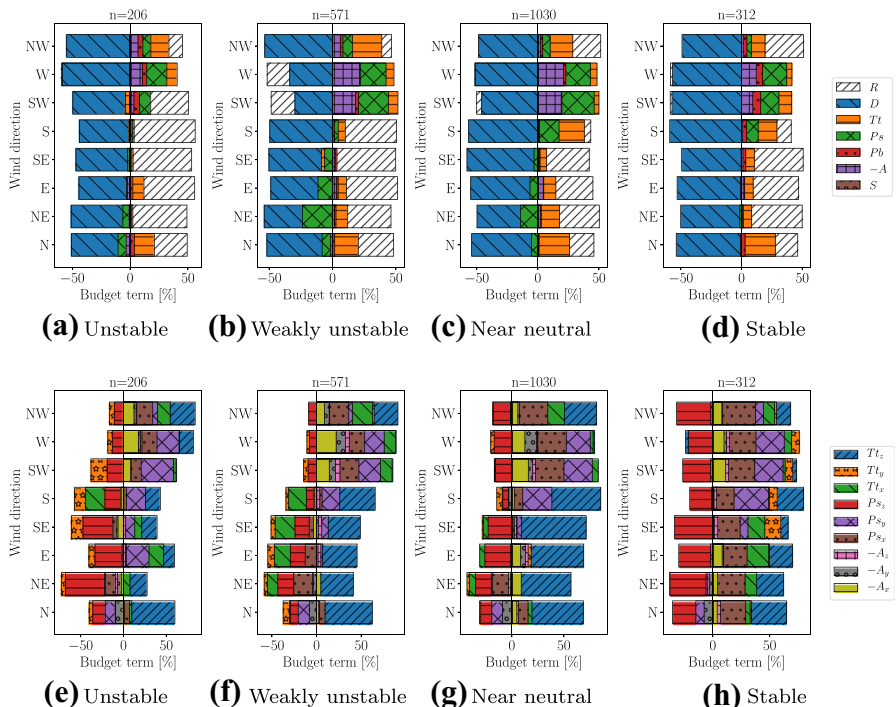


Fig. 7 Budget of k under different thermal stability conditions; budget apportioned according to terms described in Eq. 8 **a, b, c, d**; directional terms in the budget decomposed into the cross-canyon direction (x), the along-canyon direction (y), and the vertical direction (z) **e, f, g, h**; budget normalized using the sum of magnitude of all budget terms; wind direction with respect to the canyon north; classification ranges specified in Sect. 2.5.3

directions for the same ranges of thermal stability parameters and wind directions. These include the negative of advection $-A$, shear production/consumption Ps , and turbulent transport Tt . The width of each bar chart is precisely 100 although the bar chart may be shifted to either positive or negative sides of the zero axis.

From the table, on average, the percent contributions of the magnitude of the residual term R under all wind directions was 33.43, 29.14, 18.77, and 23.05 % for the unstable, weakly unstable, near neutral, and stable cases, respectively. The residual term quantified here was in the same range as other studies that reported the average residual term approximately from 20% to 40% of the total budget of k [14, 32, 38]. As noted in Table 4, the high residuals result from underestimation of the magnitudes of the turbulent transport terms, since they exhibit large systematic errors compared to other terms. This provided some confidence in the methodology adopted to apportion the terms of the budget of k , based on the premise that less accurate methodologies would result in higher errors and therefore higher percent contribution from the residual term.

From the table, and setting aside the residual term, it can be seen that for all thermal stability conditions, and averaged for all wind directions, the budget terms could be listed as dissipation D , turbulent transport Tt , shear production/consumption Ps , negative of advection $-A$, buoyant production/consumption Pb , and storage S , in decreasing order of magnitude. Some of these budget terms were consistently positive or negative, regardless

Table 5 Budget of k under unstable, weakly unstable, near neutral, and stable conditions; total budget apportioned according to terms described in Eq. 8; budget normalized using the sum of magnitude of all budget terms; wind direction with respect to the canyon north; classification ranges specified in Sect. 2.5.3

Case	S	$-A$	Pb	Ps	Tt	D	R
Unstable	%	%	%	%	%	%	%
North	0.01	-3.35	3.80	-7.02	17.17	-40.26	28.39
North-east	-0.00	-0.77	1.47	-5.45	0.95	-44.63	46.73
East	-0.02	-2.30	2.44	-0.62	9.57	-41.22	43.83
South-east	0.01	-0.64	1.56	-1.46	1.12	-44.66	50.55
South	0.01	-0.19	2.33	1.21	-0.73	-42.81	52.72
South-west	0.02	3.34	4.70	9.82	-3.91	-45.52	32.69
West	0.01	10.71	3.71	17.36	8.90	-58.43	-0.88
North-west	0.01	6.91	4.16	6.89	15.64	-54.76	11.62
Average magnitude	0.01	3.53	3.02	6.23	7.25	46.54	33.43
Weakly unstable	%	%	%	%	%	%	%
North	0.00	-1.66	1.72	-6.53	18.59	-43.59	27.90
North-east	0.00	1.45	1.31	-23.65	9.21	-30.24	34.14
East	0.01	3.09	1.37	-11.43	6.66	-37.27	40.17
South-east	0.02	2.12	1.44	-6.19	-2.53	-41.45	46.26
South	0.00	0.21	1.27	3.01	5.56	-49.49	40.45
South-west	0.06	18.17	2.32	23.59	7.48	-29.66	-18.73
West	0.00	21.29	0.60	20.34	6.23	-33.77	-17.76
North-west	-0.01	6.15	2.07	7.42	23.24	-53.44	7.68
Average magnitude	0.01	6.77	1.51	12.77	9.94	39.86	29.14
Near neutral	%	%	%	%	%	%	%
North	0.01	-0.23	0.99	-4.87	24.99	-49.06	19.86
North-east	-0.03	2.34	0.40	-14.08	14.99	-35.63	32.53
East	-0.01	4.44	0.42	-6.40	9.88	-48.56	30.29
South-east	-0.01	1.21	0.58	-3.08	5.35	-54.88	34.88
South	-0.01	0.20	1.17	15.97	20.67	-56.71	5.28
South-west	0.04	19.08	0.54	26.38	3.93	-46.14	-3.89
West	0.02	21.02	1.86	20.05	5.44	-51.07	-0.54
North-west	-0.02	2.06	1.89	6.15	18.48	-48.54	22.86
Average magnitude	0.02	6.32	0.98	12.12	12.97	48.82	18.77
Stable	%	%	%	%	%	%	%
North	-0.02	-0.26	2.87	-0.72	24.95	-52.75	18.44
North-east	0.01	0.57	0.82	-1.43	6.88	-48.66	41.63
East	-0.01	1.87	0.64	-0.78	7.05	-52.23	37.42
South-east	-0.02	1.25	2.19	-0.32	7.08	-48.93	40.22
South	0.01	1.00	3.21	9.48	15.41	-59.10	11.79
South-west	-0.05	9.24	6.48	15.00	10.55	-57.18	-1.48
West	0.09	12.01	5.08	20.01	4.29	-56.77	-1.75
North-west	0.01	1.41	2.97	3.66	11.30	-48.98	31.67
Average magnitude	0.03	3.45	3.03	6.42	10.94	53.07	23.05

of the wind direction, such as the buoyant production/consumption. However, some other terms showed a clear dependence on wind direction, such as shear production/consumption, where the contribution to the budget was negative under north, north-east, east, and south-east directions, while the contribution to the budget was positive for south, south-west, west, and north-west directions (with respect to canyon north in Fig. 1). We speculate that this could be due to the position of the control volume defined by the anemometers with respect to the main canyon vortex (with axis along the street). This canyon vortex was identified for the same street canyon in a previous field campaign [6]. Note that the control volume was closer to the north-east wall (with respect to true north). When wind was approaching from south-west, west, and north-west, (with respect to the canyon north), the control volume was situated on the updraft segment of the vortex. Air parcels reaching this segment had experienced shear production of k due to sufficient interaction of the air parcel with street-canyon surfaces. On the other hand, when wind was approaching from the north-east, east, and south-east (with respect to canyon north), the control volume was situated on the downdraft segment of the vortex. Air parcels entering this segment were speculated to have been transported from the shear layer above canyon (not measured) with high levels of k , which would subsequently be lost due to shear consumption when entering the canyon. Other terms showed mixed trends for the sign given the thermal stability condition and wind direction.

From the figure, the budget analysis of the directional terms is informative in explaining the budget of k . One can note that all terms $-A$, Ps , and Tt had both positive and negative contributions to k , albeit these contributions were made from different components of each term. The greatest component of Tt was Tt_z , which was usually positive, indicative that the turbulent transport in the vertical direction transported k into the control volume, from above the control volume (perhaps the shear layer above roof level). On the other hand, Tt_x and Tt_y could be positive or negative depending on thermal stability condition and wind direction. Under unstable and weakly unstable conditions, Tt_y was negative, while under stable conditions, Tt_y was positive, suggesting that turbulent transport along-canyon reduced k from the canyon under unstable and weakly unstable conditions, while it increased k into the canyon under stable conditions. The greatest component of Ps was Ps_z , which was usually negative, suggesting a sink mechanism for k in the canyon under most thermal stability conditions and wind directions. This could be due to the complex structure of the flow inside the canyon. For instance, formation of a vortex structure was observed in the same canyon for many wind directions in a previous field campaign [6]. If the control volume is positioned below the center of such a vortex, then mean velocity gradients in the vertical direction would be negative, hence possibly explaining the negative sign of Ps_z . On the other hand, Ps_y was positive for many thermal stability conditions and wind directions, suggesting that a thin boundary layer could develop along the surface of a canyon contributing to shear production of k . Ps_x showed mixed signs, especially influenced by the thermal stability condition and wind direction. While it acted both as a source or sink of k under unstable, weakly unstable, and neutral condition, it acted as a source of k under stable conditions. The components of $-A$ played a lesser role in transport of k into and out of the canyon with a tendency of the contribution to be positive, i.e. a source for k , except for the thermally unstable condition. The vertical component of $-A_z$ was even further less in magnitude than the horizontal components $-A_x$ and $-A_y$. All considered, the combined effect of the directional components of the budget terms, $-A$, Ps , and Tt , behaved in a very complicated manner and could create, overall, sink or source mechanisms for k in the canyon given the thermal stability condition and wind direction.

The findings were in qualitative agreement or complementary to those reported by other investigators. It has been noted that compared to the shear layer above roof height, where local production/consumption terms such as shear and buoyant production/consumption can be significant, the main source term for k in the lower street canyon was the turbulent transport, which brought k into the canyon from the rooftop level [16, 38, 46] or other locations. The present study provides similar evidence, where k is transported to the control volume from locations above the control volume, possibly from roof-top shear layer (speculated but not measured). Also it was found that both the thermal stability condition and wind direction influence the apportionment of the budget. For example, although negligible in comparison to the turbulent transport term, a higher level of buoyancy production/consumption term for the along-canyon wind direction was observed in this study and elsewhere, possibly due to more turbulent heat transfer within the canyon under those wind directions [16]. Also the thermal stability condition was responsible for diurnal variation of the budget terms, such as the buoyant production/consumption, where higher values were observed during daytime thermally unstable conditions [38].

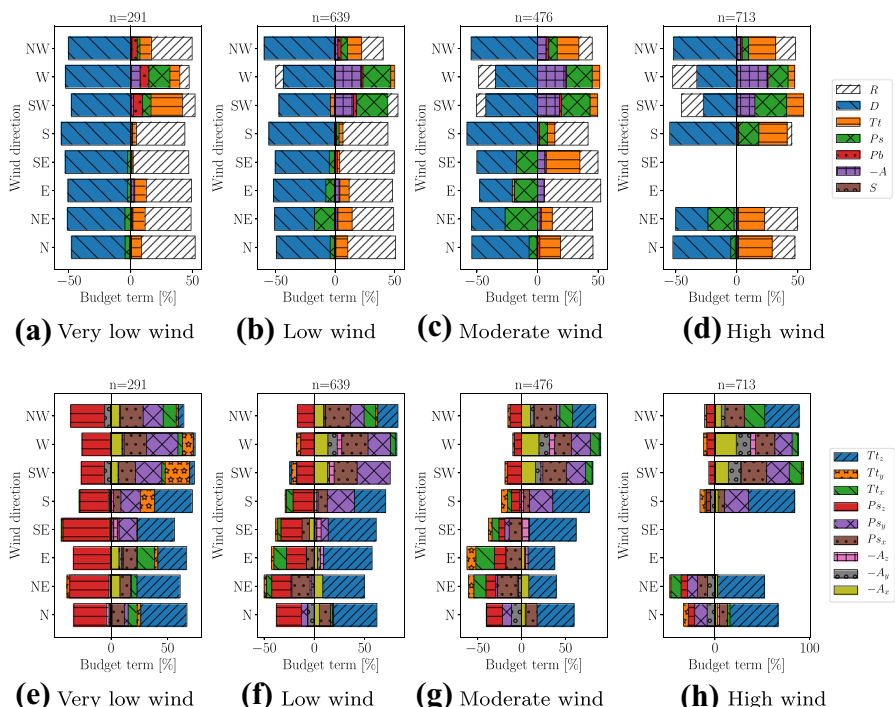


Fig. 8 Budget of k under different wind speed conditions; budget apportioned according to terms described in Eq. 8 **a, b, c, d**; directional terms in the budget decomposed into the cross-canyon direction (x), the along-canyon direction (y), and the vertical direction (z) **e, f, g, h**; budget normalized using the sum of magnitude of all budget terms; wind direction with respect to the canyon north; classification ranges specified in Sect. 2.5.3

Table 6 Budget of k under very low wind, low wind, moderate wind, and high wind conditions; total budget apportioned according to terms described in Eq. 8; budget normalized using the sum of magnitude of all budget terms; wind direction with respect to the canyon north; classification ranges specified in Sect. 2.5.3

Case	S	$-A$	Pb	Ps	Tt	D	R
Very low wind	%	%	%	%	%	%	%
North	0.00	-0.88	0.67	-3.65	8.15	-43.22	43.43
North-east	-0.02	1.19	0.61	-4.65	9.86	-46.43	37.24
East	-0.01	2.65	0.66	-2.47	9.32	-48.26	36.63
South-east	-0.00	0.41	0.74	-2.49	0.89	-50.46	45.01
South	-0.00	0.11	1.10	0.06	3.34	-56.11	39.28
South-west	-0.06	2.25	7.17	7.02	25.71	-47.80	10.00
West	0.03	7.62	7.09	17.04	8.01	-52.65	7.57
North-west	-0.00	1.00	4.31	2.16	9.35	-50.23	32.94
Average magnitude	0.02	2.01	2.79	4.94	9.33	49.39	31.51
Low wind	%	%	%	%	%	%	%
North	0.01	0.14	0.57	-4.11	9.99	-45.07	40.11
North-east	-0.01	1.80	0.65	-17.32	11.89	-33.41	34.92
East	0.01	3.37	0.64	-7.76	7.80	-43.98	36.43
South-east	0.00	0.50	1.39	-4.82	2.02	-45.43	45.84
South	0.00	0.35	0.89	2.16	3.24	-55.59	37.76
South-west	0.02	15.36	2.67	26.23	-3.90	-43.25	8.57
West	0.00	21.99	1.44	23.36	3.37	-43.42	-6.42
North-west	0.00	2.34	2.67	5.51	11.84	-59.52	18.12
Average magnitude	0.01	5.73	1.36	11.41	6.76	46.21	28.52
Moderate wind	%	%	%	%	%	%	%
North	0.02	-0.40	1.91	-6.50	17.05	-47.28	26.84
North-east	-0.01	2.17	0.94	-26.73	9.10	-27.84	33.21
East	0.00	5.41	0.31	-18.99	-1.80	-26.98	46.52
South-east	-0.04	6.03	1.16	-17.31	27.80	-32.69	14.95
South	0.00	0.29	1.29	6.67	6.08	-58.22	27.45
South-west	0.02	18.02	1.67	23.72	6.26	-42.64	-7.67
West	0.00	23.46	0.31	21.41	6.23	-34.77	-13.81
North-west	-0.01	7.10	2.18	6.98	17.89	-54.79	11.05
Average magnitude	0.01	7.86	1.22	16.04	11.53	40.65	22.69
High wind	%	%	%	%	%	%	%
North	0.01	-1.26	1.33	-3.65	27.70	-47.42	18.64
North-east	-0.01	-2.23	1.25	-21.40	21.56	-26.50	27.05
East	-	-	-	-	-	-	-
South-east	-	-	-	-	-	-	-
South	-0.01	-0.08	1.39	16.68	23.24	-54.84	3.77
South-west	0.02	14.84	-0.37	25.92	13.95	-27.08	-17.82
West	0.04	25.08	0.45	16.46	5.47	-32.71	-19.80
North-west	-0.01	3.26	1.15	5.28	22.21	-51.95	16.16
Average magnitude	0.02	7.80	0.99	16.26	19.02	40.08	17.21

3.2.3 Variation by wind speed

Figure 8 and Table 6 show the apportionment of the budget of k according to different wind speed conditions and wind directions. Again, the relevant statistic in this case was the median of each budget term for a combination of wind speed and wind direction with ranges specified in Sect. 2.5.3.

In the figure, first, in panels (a), (b), (c), and (d) the budget terms in Eq. 8 were quantified and visually demonstrated based on different ranges of wind speed and wind direction. Next, in panels (e), (f), (g), and (h), the directional components of the budget were broken down for the same ranges of wind speeds and wind directions. The percent contribution of each budget term to the total budget was calculated in the same manner as the previous section.

From the table, on average, the percent contribution of the magnitude of the residual term R under all wind directions was 31.51, 28.52, 22.69, and 17.21 % for the very low, low, moderate, and high wind conditions, respectively. It can be seen that the residual decreases with increasing wind speed, suggesting that the Reynolds decomposition approach and budget apportionment is more successful with increasing wind speed.

From the table, and setting aside the residual term, it could be seen that the relative contribution of the budget terms depended on the wind speed. For the very low wind speed condition, the budget terms could be listed as dissipation D , turbulent transport Tt , shear production/consumption Ps , buoyant production/consumption Pb , negative of advection $-A$, and storage S , in decreasing order of magnitude. For the low and moderate wind speed conditions, the budget terms could be listed as dissipation, shear production/consumption, turbulent transport, negative of advection, buoyant production/consumption, and storage, in decreasing order of magnitude. Finally, for the high wind speed condition the order was dissipation, turbulent transport, shear production/consumption, negative of advection, buoyant production/consumption, and storage. The increase in shear production/consumption, negative of advection, and turbulent transport terms with increasing wind speed can be explained by more local production/consumption of k and more effective transport of it into the urban canyon under windy conditions.

Some of these budget terms were consistently positive or negative, regardless of the wind direction, such as the buoyant production/consumption (with the exception of high wind speed condition with wind direction from the south-west). However, some other terms showed a clear dependence on wind direction, such as shear production/consumption, where the contribution to the budget was negative under north, north-east, east, and south-east directions, while the contribution to the budget was positive for south, south-west, west, and north-west directions (with respect to canyon north). A similar explanation can be provided for this as in the last section. Other terms showed mixed trends for the sign given the wind speed condition and wind direction. This behaviour was similar to what was observed under different thermal stability conditions.

From the figure, the analysis of the directional components of the terms is insightful. As seen, all budget terms $-A$, Ps , and Tt made both positive and negative contributions to the total budget, albeit these contributions were made from different components of each term. Again, the greatest component of Tt was Tt_z , which was usually positive, indicative that the turbulent transport in the vertical direction transported k into the control volume, from above the control volume (perhaps from the shear layer above roof level). On the other hand, Tt_x and Tt_y could be positive or negative depending on wind speed and wind direction. Under moderate to high wind speed conditions, Tt_y was negative, while under

very low wind speed condition, Tt_y was positive, suggesting that turbulent transport along-canyon reduced k from the canyon under moderate and high wind speed conditions, while it increased k into the canyon under very low wind speed conditions. The greatest component of Ps was Ps_z , which was usually negative, suggesting a sink mechanism for k in the canyon under most wind speed conditions and wind directions. On the other hand, Ps_y was positive for many wind speed conditions and wind directions, suggesting that a boundary layer could develop along-canyon contributing to shear production of k . Ps_x showed mixed signs, especially influenced by wind speed condition and wind direction. While it acted both as a source or sink of k under low, moderate, and high wind speed conditions, it acted as a source of k under very low wind speed conditions. The components of $-A$ played a lesser role in transport of k into and out of the canyon with a tendency of the contribution to be positive, i.e. a source for k . The vertical component of $-A_z$ was even further less in magnitude than the horizontal components $-A_x$ and $-A_y$. All considered, the combined effect of the directional components of the budget terms, $-A$, Ps , and Tt , behaved in a very confounding manner and could create, overall, sink or source mechanisms for k in the canyon given the wind speed condition and wind direction.

The findings were in overall agreement with those reported by other investigators. It has been reported that the turbulent transport term below the roof level was positive, implying downward transport of k from the rooftop shear layer and elsewhere into the urban canyon [32]. Results here also showed this overall behaviour, particularly for the vertical component of turbulent transport, which dominated the horizontal components. As stated earlier, the transport terms in the lower street canyon ought to be larger than other production/consumption terms [16, 38, 46]. The findings here confirmed this although the shear production/consumption term was also found to make a high positive contribution under moderate and high wind speed conditions for certain wind directions.

3.3 Thermal imaging at canyon and neighborhood scales

Before the analysis of the heat budget, it is insightful to study the surface temperatures at the street-canyon and neighborhood scales, as such analysis will provide physical explanations for the behavior of the heat budget terms. The surface temperature observations were on selected, but representative, days, so the subsequent interpretations can be understood as being approximate. The results for surface temperature analysis at the street-canyon scale were visualized in Aliabadi et al. [6] and are not reproduced here for brevity. These observations corresponded to conditions representative of clear skies with moderate wind speed conditions. The top of north-east and south-west walls (with respect to true north) experienced a temperature difference by up to 10 K as a function of diurnal time, where the south-west wall exhibited higher temperatures than the north-east wall (with respect to true north) from sunrise to noon LST, while the south-west wall exhibited lower temperatures than the north-east wall (with respect to true north) from noon LST to sunset. The top and bottom of each wall also experienced a temperature difference up to 5 K. These observations were in agreement with those performed by Offerle et al. [40] and Santamouris et al. [51]. The difference between grass and asphalt surface temperatures at street level during the day was as much as 10 K, with the grass being cooler than the asphalt.

Figure 9 shows the areal view of land surface temperatures at neighborhood scale at 50 m × 50 m horizontal resolution. The mean surface temperature in each tile is shown for four-hourly observation windows of 0400–0800, 0800–1200, 1200–1600, 1600–2000, and 2000–2400 LST. During 1200–1600 and 1600–2000 LST, warm surface

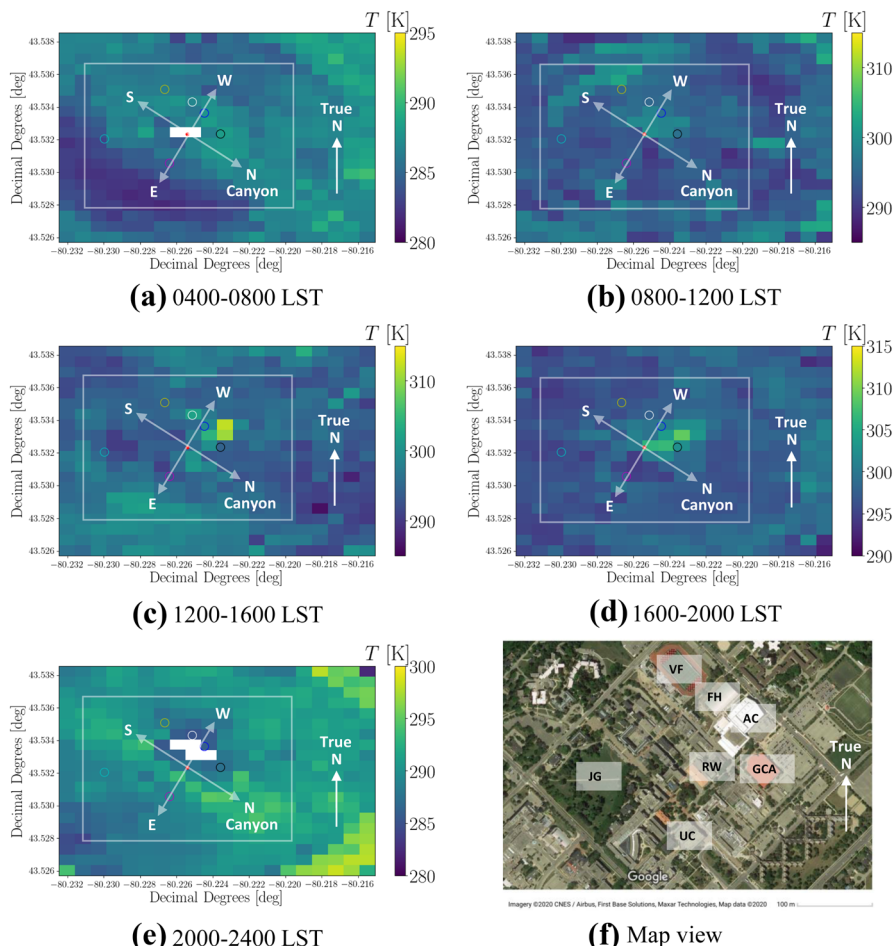


Fig. 9 Areal view of land surface temperature at 50 m × 50 m horizontal resolution measured by the Tethered Air Blimp (TAB); **a** 0400–0800 LST; **b** 0800–1200 LST; **c** 1200–1600 LST; **d** 1600–2000 LST; **e** 2000–2400 LST; **f** map view of major campus areas and buildings specified using a white inset in panels **a–e** showing the Reek Walk (RW: red circles in panels **a–e**), Gryphon Centre Arena (GCA: black circles in panels **a–e**), University Centre (UC: magenta circles in panels **a–e**), Athletic Centre (AC: blue circles in panels **a–e**), Varsity Field (VF: yellow circles in panels **a–e**), Johnston Green (JG: cyan circles in panels **a–e**), and Field House (FH: white circles in panels **a–e**); times in Local Standard Time (LST = UTC - 5)

temperatures on the north-west of the street canyon were observed (with respect to canyon north), where surface temperatures were higher than the surroundings by ~ 10 K. These warm surfaces are associated with impervious surfaces (parking lot) and large energy consuming buildings (Athletic Centre (AC) and Gryphon Centre Arena (GCA), which is an ice hockey arena). During 2000–2400 LST slightly warmer temperatures were noted on the east of the street canyon (with respect to canyon north), where surface temperatures were higher than the surroundings by ~ 5 K. We speculate that this behaviour was related to the different land use conditions and morphometric parameters on the east and west sides of the street canyon (with respect to canyon north). On the west

side of the canyon (with respect to canyon north), the mainly large impervious surfaces gained higher temperatures (compared to the surroundings) with abundance of incoming solar shortwave radiation during midday and reached lower temperatures with long-wave radiation loss at nighttime. On the other hand, on the east side of the canyon (with respect to canyon north), the built-up areas with vegetation gained lower temperatures (compared to the surroundings) due to shading and evapotranspiration during daytime and reached higher temperatures due to radiation trapping at nighttime. Morphometric parameters support this speculation. Averaged over north-east, east, and south-east direction (with respect to canyon north) the mean building height and frontal area density are $\bar{H} = 16$ m and $\lambda_f = 0.17$, respectively, while averaged over south west, west, and north-west directions (with respect to canyon north) the corresponding values are $\bar{H} = 11.3$ m and $\lambda_f = 0.12$, respectively. Note that thermal images at very oblique angles associated with locations too far from the street canyon (where TAB was launched) did not provide accurate measurements of the surface temperatures.

3.4 Heat budget

3.4.1 Diurnal variation

Similar to k , it is informative to study the diurnal variation of the terms in the budget of heat before the analysis of the budget terms classified per stability parameter, wind speed, and wind direction. Figure 10 shows the medians of the budget terms as they varied diurnally. These statistics were calculated based on all observations at the same hour.

Again, the storage term S was two orders of magnitude smaller than other terms, so it could be assumed that Θ met the quasi-statistically-stationary condition. Although not being directly measured, the storage term in a previous study was suggested to be mainly proportional to the flux divergence term [46]. The other two terms in the budget,

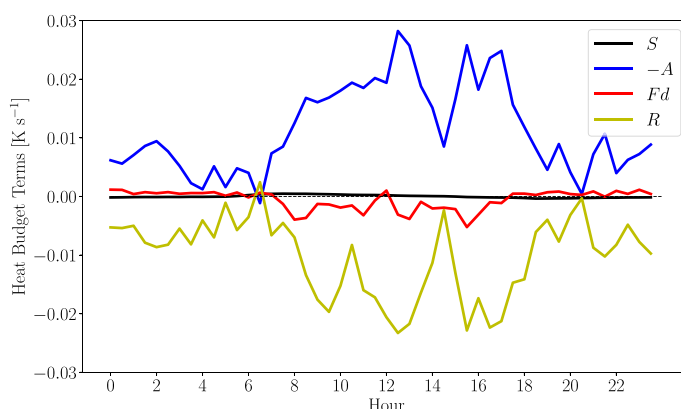


Fig. 10 Diurnal variation of terms in the budget of heat; budget apportioned according to terms described in Eq. 10; the medians are shown for every half hour period; times are in Local Standard Time (LST = UTC - 5)

i.e. the negative of advection term $-A$ and the flux divergence term F_d , seemed to be two orders of magnitude larger than the storage term and seemed to balance each other, particularly during the daytime thermally unstable condition. In contrast to the previous speculation by Ramamurthy et al. [46], it is reasonable to suggest that the advection term was more important than the storage term in balancing the budget. Nevertheless, a great portion of the budget was still apportioned as the residual R because it was not possible to estimate the other terms using the methodology of this study.

3.4.2 Variation by thermal stability

Figure 11 and Table 7 show the apportionment of the budget of $\bar{\Theta}$ according to Eq. 10 for different thermal stability parameters and wind directions. Again, the median of each budget term was used for a combination of thermal stability parameter and wind direction with ranges specified in Sect. 2.5.3. The budget contributions [% C], for either the total budget or the budget associated with directional terms, are presented as the percent contribution of the median of each term to the summation of the magnitude of the median of all terms, i.e.

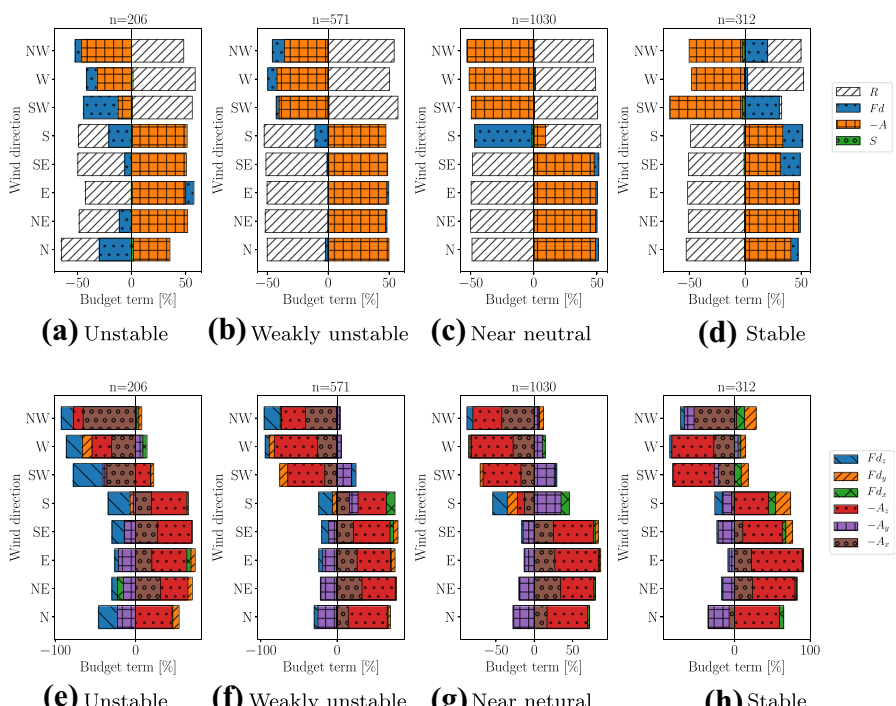


Fig. 11 Budget of heat under different thermal stability conditions; budget apportioned according to terms described in Eq. 10 **a, b, c, d**; directional terms in the budget decomposed into the cross-canyon direction (x), the along-canyon direction (y), and the vertical direction (z) **e, f, g, h**; wind direction with respect to the canyon north

Table 7 Budget of heat under unstable, weakly unstable, near neutral, and stable conditions; total budget apportioned according to terms described in Eq. 10; budget normalized using the sum of magnitude of all budget terms; wind direction with respect to the canyon north; classification ranges specified in Sect. 2.5.3

Case	<i>S</i>	<i>-A</i>	<i>Fd</i>	<i>R</i>
Unstable	%	%	%	%
North	2.09	33.42	-29.53	-34.97
North-east	0.26	51.63	-11.03	-37.08
East	0.80	49.27	7.57	-42.36
South-east	0.22	50.43	-6.09	-43.27
South	0.92	50.43	-20.79	-27.86
South-west	1.04	-12.18	-31.73	55.04
West	1.48	-31.27	-9.94	57.31
North-west	0.22	-45.80	-5.94	48.04
Average magnitude	0.88	40.55	15.33	43.24
Weakly unstable	%	%	%	%
North	0.17	49.75	-2.20	-47.88
North-east	0.02	47.16	1.09	-51.73
East	0.18	48.00	1.60	-50.22
South-east	0.45	48.42	-0.94	-50.18
South	0.37	47.05	-10.86	-41.72
South-west	0.68	-40.32	-2.35	56.65
West	0.26	-42.01	-7.65	50.07
North-west	0.10	-35.80	-9.99	54.11
Average magnitude	0.28	44.81	4.59	50.32
Near neutral	%	%	%	%
North	-0.15	48.83	2.25	-48.77
North-east	-0.13	48.83	1.18	-49.86
East	-0.06	49.06	1.33	-49.55
South-east	-0.17	47.74	3.72	-48.36
South	-1.53	9.38	-45.51	43.58
South-west	-0.20	-49.31	0.56	49.93
West	-0.28	-50.87	1.25	47.60
North-west	-0.55	-51.92	-0.45	47.08
Average magnitude	0.38	44.49	7.03	48.09
Stable	%	%	%	%
North	-0.83	40.78	6.45	-51.94
North-east	-0.63	47.71	1.40	-50.26
East	-0.40	47.96	0.56	-51.08
South-east	-1.09	31.24	17.91	-49.76
South	-1.09	33.56	17.61	-47.74
South-west	-2.48	-65.02	30.40	2.10
West	-0.62	-47.31	2.07	50.00
North-west	-2.29	-47.85	19.94	29.92
Average magnitude	1.18	45.18	12.04	41.60

$$\%C = \frac{100 \times \text{Budget term}}{|S| + |-A| + |Fd| + |R|}, \quad (14)$$

$$\%C = \frac{100 \times \text{Budget term}}{|-A_x| + |-A_y| + |-A_z| + |Fd_x| + |Fd_y| + |Fd_z|}, \quad (15)$$

respectively. In the figure, first, in panels (a), (b), (c), and (d) the budget terms in Eq. 10 were quantified and visually demonstrated based on different ranges of thermal stability parameter and wind direction. Next, in panels (e), (f), (g), and (h), the directional components of the budget were broken down along the x (cross-canyon), y (along-canyon), and z (vertical) directions for the same ranges of thermal stability parameters and wind directions. These include the negative of advection $-A$ and flux divergence Fd .

According to the table, on average, the percent contribution of the magnitude of the residual term R under all wind directions was 43.24, 50.32, 48.09, and 41.60 % for the unstable, weakly unstable, near neutral, and stable cases, respectively. The unexplained portion of the budget is typically high and on average from 41.60 to 50.32 %. The breakdown of the residual for each wind direction also indicates that a large portion of the budget is unaccounted. This is likely due to limited measurements that did not permit apportionment of all budget terms. However, there was one anomaly; under the thermally stable case and wind from the south-west direction, the percent contribution of the residual was very low, while that of the flux divergence was very high. This could be explained with the aid of Fig. 5 showing that the frequency of high wind speed observations from the south-west direction could be high during 0000–0400 and 0400–0800 LST, coincident with the thermally stable case. With higher wind speeds the Reynolds decomposition approach was more successful, where a greater portion of the budget could be explained.

From the table, and setting aside the residual term, it can be seen that for all thermal stability conditions and averaged for all wind directions, the budget terms could be listed as negative of advection $-A$, flux divergence Fd , and storage S , in decreasing order of magnitude, with negative of advection dominating the other two terms. The negative of advection term had a clear dependence on wind direction. It was consistently positive for north, north-east, east, south, and south-east directions (with respect to canyon north), while it was consistently negative for south-west, west, and north-west directions (with respect to canyon north). The flux divergence term, on the other hand, acted as a balancing term for the negative of advection, with opposite signs for many wind directions, although occasionally mixed trends for the sign could be observed given the thermal stability condition and wind direction.

From the figure, the analysis of the directional components of the budget is informative in explaining the budget of Θ . The individual budget terms of Fd and $-A$ made both positive and negative contributions that were strongly influenced by wind direction. The greatest components of Fd were Fd_z and Fd_y , possibly due to existence of large gradients of temperature in the vertical and along-canyon directions. The components of $-A$ played a more important role in transport of heat into and out of the canyon, and they each showed a strong dependence on wind direction. The balance between the advective and flux divergence terms can be explained using the visualization provided in Fig. 12, showcasing two scenarios where wind was from the east and west of the canyon (with respect to canyon north). Surface temperatures at the neighborhood scale suggested that under thermally unstable condition (1200–1600 and 1600–2000 LST) the advection term along the canyon ($-A_y$) could transport heat from areas with higher surface temperatures associated

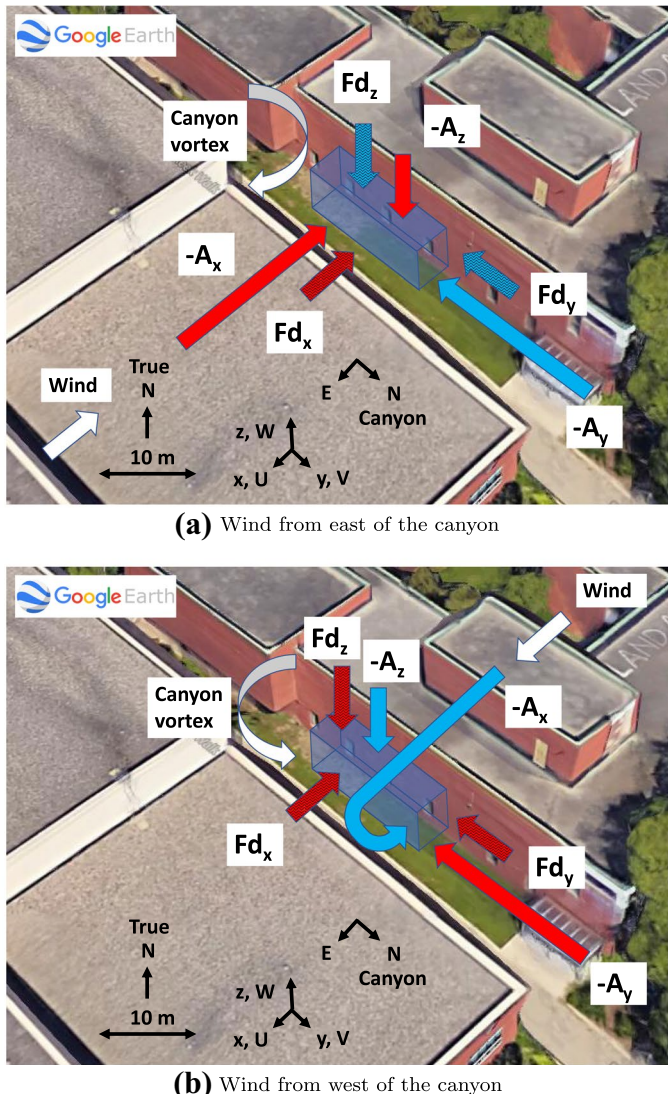


Fig. 12 Visualization of the advective and flux divergence terms in heat Eq. 10; **a** wind from the east of the canyon, with respect to the canyon north; **b** wind from the west of the canyon, with respect to the canyon north; positive terms shown in red and negative terms shown in blue according to Fig. 11e; advective terms filled with solid color and flux divergence terms filled with hatched color

with impervious surfaces and large energy-consuming buildings in the neighborhood (see Fig. 9c,d), where $-A_y$ was positive associated with the south-west, west, and north-west directions (with respect to canyon north), while it was negative for south-east, east, and north-east directions (with respect to canyon north). On the other hand, advection terms across the canyon ($-A_x$) and in the vertical direction ($-A_z$) suggested that air masses coming from the south-east, east, and north-east of the canyon (with respect to canyon north) made a positive contribution to the budget, while air masses coming from the south-west,

west, and north-west of the canyon (with respect to canyon north) made a negative contribution to the budget under all stability conditions. We can note that on the east side of the canyon (with respect to canyon north), the building mechanical system and heat rejection are positioned on the roof of the Rozanski Hall (see Fig. 1b), possibly explaining the positive contribution of the $-A_x$ and $-A_z$ terms to the heat budget when wind was coming from the south-east, east, and north-east directions (with respect to canyon north). Also since the control volume was closer to the north-east wall (with respect to true north), the air mass approaching the control volume entered the downdraft segment of the main canyon vortex (with its axis along canyon) directly as it left the shear layer above (speculated but not measured), thus advecting warm air into the control volume. On the other hand, on the west side of the canyon (with respect to canyon north), the green space and court yard associated with the Landscape and Architecture building transported cooler air into the canyon when wind was coming from the south-west, west, and north-west directions (with respect to canyon north), possibly explaining the negative contribution of the $-A_x$ and $-A_z$ terms to the heat budget. Also since the control volume was closer to the north-east wall (with respect to true north), the air mass approaching the control volume entered the updraft segment of the main canyon vortex (with its axis along canyon) possibly after interaction with canyon grass at lower temperatures, thus advecting cool air into the control volume. It must be noted that the differential canyon wall temperatures occurred during the daytime (thermally unstable condition) as explained in Sect. 3.3. For the thermally unstable condition, according to Fig. 5c,d, there was similar frequencies of wind directions from the eastern or western sectors (with respect to canyon north) during 0800–1200 LST (when the south-west wall temperature was higher than the north-east wall temperature (with respect to true north)) and 1200–1600 LST (when the north-east wall temperature was higher than the south-west wall temperature (with respect to true north)). Therefore, the effect of the differential canyon wall temperatures could not be observed or quantified. All considered, the combined effect of the directional components of the budget terms, F_d and $-A$, show a strong dependence on wind direction.

There is a paucity of field observations of the heat budget terms within the urban RSL by other investigators. The findings here suggested that beside the flux divergence term, the advection term was also a major contributor for the transport of heat both in the vertical and horizontal directions at all thermal stability conditions and wind directions. Furthermore, the sign of the advection term was strongly linked to the wind direction. When positive, the advection mechanism transported warm air into the urban canyon, while, when negative, it transported cool air into the urban canyon. The results also showed that a great portion of the budget terms was unexplained, due to the current limitations of this study in quantifying more budget terms, as opposed to the presence of random and systematic errors as well as errors due to finite differencing to calculate spatial derivatives. This later point is inferred because the estimated residual error in Table 4 is lower than the observed percent contribution of the residual term. Overall, the budget terms for heat responded more significantly to changing of wind direction, rather than the change in thermal stability.

3.4.3 Variation by wind speed

Figure 13 and Table 8 show the apportionment of the budget of $\bar{\Theta}$ according to different wind speed conditions and wind directions. Again, the relevant statistic in this case was

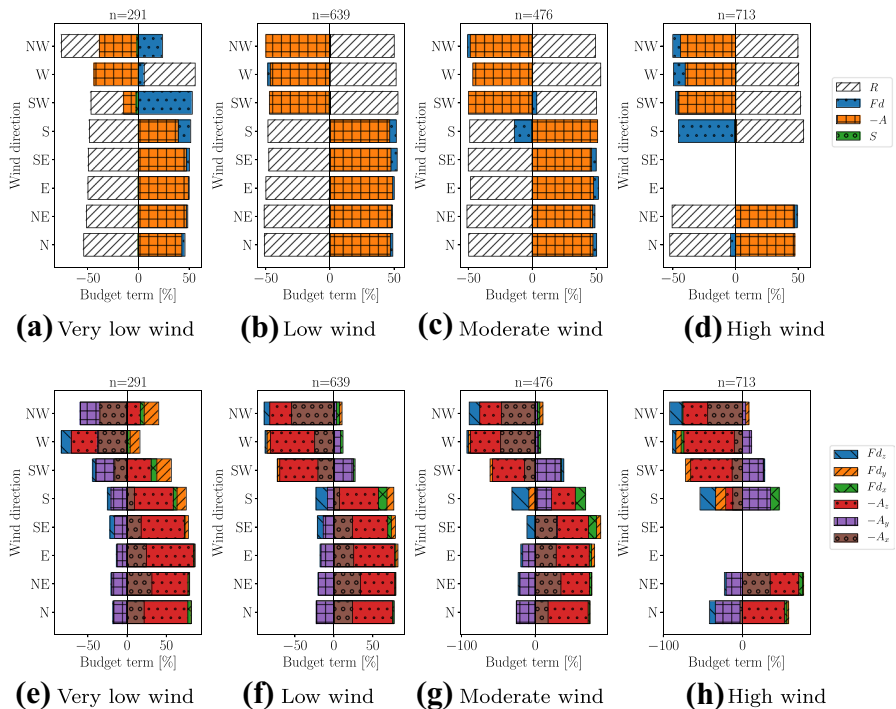


Fig. 13 Budget of heat under different turbulence conditions; budget apportioned according to terms described in Eq. 10 a, b, c, d; directional terms in the budget decomposed into the cross-canyon direction (x), the along-canyon direction (y), and the vertical direction (z) e, f, g, h; wind direction with respect to the canyon north

the median of each budget term for a combination of wind speed and wind direction with ranges specified in Sect. 2.5.3.

In the figure, first, in panels (a), (b), (c), and (d) the budget terms in Eq. 10 were quantified and visually demonstrated based on different ranges of wind speed and wind direction. Next, in panels (e), (f), (g), and (h), the directional components of the budget were broken down for the same ranges of wind speeds and wind directions. The percent contribution of each budget term to the total budget was calculated in the same manner as the previous section.

From the table, on average, the percent contribution of the magnitude of the residual term R under all wind directions was 46.56, 50.15, 47.91, and 50.8 % for the very low, low, moderate, and high wind speed conditions, respectively.

From the figure, and setting aside the residual term, it can be seen that the negative of advection $-A$ term dominated the flux divergence Fd and storage S terms. The sign of $-A$ showed a strong dependence on wind direction similar to the observations in the previous section. Also the opposite sign between $-A$ and Fd for many wind directions indicated that advection and flux divergence terms balanced each other.

From the figure, the analysis of the directional components of the budget revealed similar apportionment to the previous section. The individual budget terms of Fd and $-A$ made both positive and negative contributions that were strongly influenced by wind

Table 8 Budget of heat under very low wind, low wind, moderate wind, and high wind conditions; total budget apportioned according to terms described in Eq. 10; budget normalized using the sum of magnitude of all budget terms; wind direction with respect to the canyon north; classification ranges specified in Sect. 2.5.3

Case	<i>S</i>	<i>-A</i>	<i>Fd</i>	<i>R</i>
Very low wind	%	%	%	%
North	−0.39	42.87	3.05	−53.70
North-east	−0.25	47.62	1.07	−51.06
East	−0.28	49.41	0.68	−49.64
South-east	0.10	47.23	3.13	−49.54
South	−0.13	39.39	12.23	−48.26
South-west	−2.35	−12.27	53.12	−32.26
West	−0.16	−43.84	5.68	50.32
North-west	−1.44	−37.02	23.86	−37.68
Average magnitude	0.64	39.96	12.85	46.56
Low wind	%	%	%	%
North	−0.22	47.10	1.93	−50.75
North-east	−0.05	48.09	0.73	−51.12
East	0.17	48.78	1.19	−49.85
South-east	0.10	47.50	4.82	−47.59
South	0.16	46.47	5.12	−48.25
South-west	−0.50	−46.47	0.51	52.52
West	−0.13	−46.27	−2.00	51.60
North-west	−0.03	−49.84	0.60	49.54
Average magnitude	0.17	47.56	2.11	50.15
Moderate wind	%	%	%	%
North	0.01	47.39	2.85	−49.74
North-east	−0.04	47.13	1.79	−51.05
East	0.01	47.91	3.74	−48.34
South-east	−0.03	46.40	3.55	−50.02
South	−0.34	51.07	−13.72	−34.86
South-west	−0.06	−49.85	3.50	46.59
West	0.14	−46.50	0.09	53.27
North-west	−0.06	−48.42	−2.09	49.43
Average magnitude	0.09	48.09	3.92	47.91
High wind	%	%	%	%
North	0.15	47.31	−3.92	−48.63
North-east	−0.06	47.14	2.21	−50.59
East	−	−	−	−
South-east	−	−	−	−
South	−0.79	0.87	−44.83	53.51
South-west	0.20	−45.83	−2.12	51.85
West	0.33	−40.20	−9.37	50.10
North-west	−0.02	−43.98	−6.08	49.92

Table 8 (continued)

High wind	%	%	%	%
Average magnitude	0.26	37.6	11.4	50.8

direction. The greatest components of Fd were Fd_z and Fd_y , with Fd_z being usually negative, indicating that the turbulent transport in the vertical direction usually removed heat from the canyon, although some exceptions were noted when Fd_z was positive. Fd_x and Fd_y could be positive or negative depending on the wind speed and wind direction. The components of $-A$ played a more important role in transport of heat into and out of the canyon, and they all showed a strong dependence on wind direction. The components $-A_x$ and $-A_z$ exhibited the same sign for a given wind speed and wind direction. They were negative for the south-west, west, and north-west directions, while they were positive for the south-east, east, and north-east directions (with respect to canyon north). Same arguments can be put forward in explaining this phenomenon as in the previous section. All considered, the combined effect of the directional components of the budget terms, Fd and $-A$, show a strong dependence on wind direction.

Again, due to lack of field observations of the heat budget terms within the urban RSL, the findings here could not be directly compared to those of other investigators. The findings, again, indicated the important role of advective transport of heat within the urban RSL along with the flux divergence transport. Overall, the budget terms for heat responded more significantly to changing of wind direction, rather than the change in wind speed.

4 Conclusions and future work

This study quantified and analyzed the budget terms of turbulence kinetic energy k and heat in the urban roughness sublayer (RSL) using field observations. The observations were conducted in the Reek Walk, inside a quasi two-dimensional urban canyon located at the University of Guelph, Guelph, Canada, from 15 July 2018 to 5 September 2018. The budget terms were analyzed under four stability classes, from thermally unstable to stable conditions, as well as under four wind speed conditions, from very low to high wind conditions. The budget terms were further analyzed under varying wind directions in eight sectors with respect to the canyon axis. In total 2119 data records were analyzed, which were measured for 30 min each, for a total of 1059.5 hr of observations.

4.1 Turbulence kinetic energy budget

The diurnal variation of the budget terms of k indicated that the storage term was two orders of magnitude smaller than other terms, so it could be assumed that k met the quasi-statistically-stationary condition. The advection term had the tendency to be positive during daytime, making a contribution to increase k by transporting it from locations with higher intensities of k such as the shear layer above roof height (speculated but not measured). The buoyant production/consumption term was lower in magnitude compared to other budget terms, but it had the tendency to be positive at most diurnal times. The remaining budget terms of shear production/consumption, turbulent transport, and dissipation were greater in magnitude than the storage, advection, and buoyant production/consumption terms, but they appeared to balance one another. During daytime, it appeared that

turbulent transport relocated k into the canyon from locations with higher intensities of k , such as the shear layer above roof height (speculated but not measured), while shear production/consumption and dissipation balanced it.

The apportionment of the budget terms of k according to thermal stability condition indicated that compared to the shear layer above roof height (speculated but not measured), where local production/consumption terms such as shear and buoyant production/consumption can be significant, the main source term for k in the lower street canyon was the turbulent transport term, which relocated k into the canyon from the rooftop level. Also it was found that the thermal stability condition influenced the apportionment of the budget. Although negligible in comparison to the turbulent transport term, a higher level of buoyancy production/consumption term for the along-canyon wind direction was observed in this study and elsewhere, possibly due to more turbulent heat transfer within the canyon under those wind directions. Also the thermal stability condition was responsible for diurnal variation of the budget terms, such as the buoyant production/consumption, where higher values were observed during daytime thermally unstable conditions.

The apportionment of the budget terms of k according to the wind speed condition indicated that the turbulent transport term below the roof level was positive, implying downward transport of k from the rooftop shear layer (speculated but not measured) into the urban canyon. This hypothesis was re-enforced, particularly given the vertical component of turbulent transport, which dominated the horizontal components. The transport terms in the lower street canyon were larger than other production/consumption terms although the shear production/consumption term was also found to make a high positive contribution under moderate and high wind speed conditions for certain wind directions.

4.2 Heat budget

The diurnal variation of the budget terms of heat also indicated that the storage term was two orders of magnitude smaller than other terms, so it could be assumed that Θ met the quasi-statistically-stationary condition. The other two terms in the budget, the advection term and the flux divergence term, seemed to be two orders of magnitude larger than the storage term and appeared to balance one another, particularly during the daytime thermally unstable condition. While not being quantified in previous studies, it is reasonable to suggest that the advection term was more important than the storage term in balancing the budget. Nevertheless, a great portion of the budget was still apportioned as the residual because other terms of the budget were not estimated using the methodology of this study.

The apportionment of the budget terms of heat according to thermal stability condition suggested that beside the flux divergence term, the advection term was also a major contributor to transport of heat both in the vertical and horizontal directions at all thermal stabilities and wind directions. Furthermore, the sign of the advection term was strongly linked to the wind direction. When positive, the advection mechanism transported warm air into the urban canyon, while, when negative, it transported cool air into the urban canyon. This was linked to the morphology and land use differences surrounding the urban canyon.

The apportionment of the budget terms of heat according to the wind speed indicated the important role of advective transport of heat within the urban RSL along with the flux divergence transport.

4.3 Implications

While previous studies attempted to apportion the budget of k using laboratory or field observations, very few studies have attempted to apportion the budget of heat using either laboratory or field observations in the urban RSL. This study filled this gap. In addition, this study provided a complementary approach by provisioning measurement locations spanned in all three coordinate directions with respect to the urban canyon to quantify the budget terms rigorously. This approach excluded the need for assuming horizontal homogeneity of meteorological conditions in the urban RSL, and neither did it require quantification of dispersive terms of transport. This study resulted in more detailed quantification of the budget terms for both k and heat. In addition, it was found that the advective terms in both the k and heat transport equations made a measurable contribution to the budgets and could not be ignored neither in the horizontal nor vertical directions. Currently, many modelling methodologies, particularly those based on the one-dimensional vertical diffusion [29, 33, 34, 50], may overlook this important mode of transport. Based on the evidence provided in this study, it is imperative that such modes of transport be accounted for in models, particularly those attempting to resolve the meteorological variables at microscale.

4.4 Future work

Future observations of the budget terms of turbulence kinetic energy and heat in the urban roughness surface layer should extend to other urban configurations, different climate zones, and different seasons. Different urban configurations may involve various plan area and frontal area densities, urban surface properties (hydrological, radiative, aerodynamic, and thermal properties), building types, vegetation type, and cover fraction. In addition, future apportionment of the budget terms of the heat equation requires more detailed quantification of radiative flux divergence and latent heat terms. Finally, more sensors (greater than 3) can be arrayed in all three coordinate directions to quantify the budget terms with less error due to finite differencing in the calculation of spatial derivatives.

Acknowledgements The authors thank the assistance of Benjamin Dyer for field observation data collection and organization. The assistance of William D. Lubitz is appreciated for lending extra ultrasonic anemometers to the authors. The authors are indebted to Steve Nyman, Chris Duiker, Peter Purvis, Manuela Racki, Jeffrey Defoe, Joanne Ryks, Ryan Smith, James Bracken, and Samantha French at the University of Guelph, who helped with the campaign logistics. Special credit is directed toward Amanda Sawlor, Datev Dodkelian, Esra Mohamed, Di Cheng, Randy Regan, Margaret Love, and Angela Vuk at the University of Guelph for administrative support. The computational platforms were set up with the assistance of Jeff Madge, Joel Best, and Matthew Kent at the University of Guelph. This work was supported by the University of Guelph, Ed McBean philanthropic fund, the Discovery Grant program (401231) from the Natural Sciences and Engineering Research Council (NSERC) of Canada; Government of Ontario through the Ontario Centres of Excellence (OCE) under the Alberta-Ontario Innovation Program (AOIP) (053450); and Emission Reduction Alberta (ERA) (053498). OCE is a member of the Ontario Network of Entrepreneurs (ONE).

References

1. Ahmadi-Baloutaki M, Aliabadi AA (2021) A very large-eddy simulation model using a reductionist inlet turbulence generator and wall modeling for stable atmospheric boundary layers. *Fluid Dyn* 56:413–432. <https://doi.org/10.1134/S0015462821020026>

2. Aliabadi AA (2018) Theory and applications of turbulence: A fundamental approach for scientists and engineers. Amir A. Aliabadi Publications, Guelph, Ontario, Canada
3. Aliabadi AA, Staebler RM, Liu M, Herber A (2016) Characterization and parametrization of Reynolds stress and turbulent heat flux in the stably-stratified lower Arctic troposphere using aircraft measurements. *Bound-Lay Meteorol* 161(1):99–126. <https://doi.org/10.1007/s10546-016-0164-7>
4. Aliabadi AA, Krayenhoff ES, Nazarian N, Chew LW, Armstrong PR, Afshari A, Norford LK (2017) Effects of roof-edge roughness on air temperature and pollutant concentration in urban canyons. *Bound-Lay Meteorol* 164(2):249–279. <https://doi.org/10.1007/s10546-017-0246-1>
5. Aliabadi AA, Veriotis N, Pedro G (2018) A Very Large-Eddy Simulation (VLES) model for the investigation of the neutral atmospheric boundary layer. *J Wind Eng Ind Aerodyn* 183:152–171. <https://doi.org/10.1016/j.jweia.2018.10.014>
6. Aliabadi AA, Moradi M, Clement D, Lubitz WD, Gharabaghi B (2019) Flow and temperature dynamics in an urban canyon under a comprehensive set of wind directions, wind speeds, and thermal stability conditions. *Environ Fluid Mech* 19(1):81–109. <https://doi.org/10.1007/s10652-018-9606-8>
7. Balogun AA, Tomlin AS, Wood CR, Barlow JF, Belcher SE, Smalley RJ, Lingard JJN, Arnold SJ, Dobre A, Robins AG, Martin D, Shaller DW (2010) In-street wind direction variability in the vicinity of a busy intersection in central London. *Bound-Lay Meteorol* 136(3):489–513. <https://doi.org/10.1007/s10546-010-9515-y>
8. Barlow JF, Haliotis CH, Lane SE, Wood CR (2015) Observations of urban boundary layer structure during a strong urban heat island event. *Environ Fluid Mech* 15(2):373–398. <https://doi.org/10.1007/s10652-014-9335-6>
9. Blackman K, Perret L, Savory E, Piquet T (2015) Field and wind tunnel modeling of an idealized street canyon flow. *Atmos Environ* 106:139–153. <https://doi.org/10.1016/j.atmosenv.2015.01.067>
10. Blackman K, Perret L, Calmet I, Rivet C (2017) Turbulent kinetic energy budget in the boundary layer developing over an urban-like rough wall using PIV. *Phys Fluids* 29:085113. <https://doi.org/10.1063/1.4997205>
11. Blackman K, Perret L, Calmet I (2018) Energy transfer and non-linear interactions in an urban boundary layer using Stochastic Estimation. *J Turbul* 19(10):849–867. <https://doi.org/10.1080/14685248.2018.1520996>
12. Böhm M, Finnigan JJ, Raupach MR, Hughes D (2013) Turbulence structure within and above a canopy of bluff elements. *Bound-Lay Meteorol* 146(3):393–419. <https://doi.org/10.1007/s10546-012-9770-1>
13. Byerlay RAE, Nambiar MK, Nazem A, Nahian MR, Biglarbegian M, Aliabadi AA (2020) Measurement of land surface temperature from oblique angle airborne thermal camera observations. *Int J Remote Sens* 41(8):3119–3146. <https://doi.org/10.1080/01431161.2019.1699672>
14. Castro IP, Cheng H, Reynolds R (2006) Turbulence over urban-type roughness: Deductions from wind-tunnel measurements. *Bound-Lay Meteorol* 118(1):109–131. <https://doi.org/10.1007/s10546-005-5747-7>
15. Chew LW, Aliabadi AA, Norford LK (2018) Flows across high aspect ratio street canyons: Reynolds number independence revisited. *Environ Fluid Mech* 18:1275–1291. <https://doi.org/10.1007/s10652-018-9601-0>
16. Christen A, Rotach MW, Vogt R (2009) The budget of turbulent kinetic energy in the urban roughness sublayer. *Bound-Lay Meteorol* 131(2):193–222. <https://doi.org/10.1007/s10546-009-9359-5>
17. Finnigan J (2000) Turbulence in plant canopies. *Annu Rev Fluid Mech* 32(1):519–571. <https://doi.org/10.1146/annurev.fluid.32.1.519>
18. Giometto MG, Christen A, Meneveau C, Fang J, Krafczyk M, Parlange MB (2016) Spatial characteristics of roughness sublayer mean flow and turbulence over a realistic urban surface. *Bound-Lay Meteorol* 160(3):425–452. <https://doi.org/10.1007/s10546-016-0157-6>
19. Grimmond CSB, Oke TR (1999) Aerodynamic properties of urban areas derived from analysis of surface form. *J Appl Meteorol* 38(9):1262–1292
20. Höglström U (1988) Non-dimensional wind and temperature profiles in the atmospheric surface layer: A re-evaluation. *Bound-Lay Meteorol* 42:55–78. <https://doi.org/10.1007/BF00119875>
21. Inagaki A, Kanda M (2010) Organized structure of active turbulence over an array of cubes within the logarithmic layer of atmospheric flow. *Bound-Lay Meteorol* 135(2):209–228. <https://doi.org/10.1007/s10546-010-9477-0>
22. Kaimal JC, Finnigan JJ (1994) Atmospheric boundary layer flow, Their structure and measurement. Oxford University Press, Oxford
23. Kanda M, Moriizumi T (2009) Momentum and heat transfer over urban-like surfaces. *Bound-Lay Meteorol* 131:385–401. <https://doi.org/10.1007/s10546-009-9381-7>

24. Kanda M, Kawai T, Kanega M, Moriwaki R, Narita K, Hagishima A (2005) A simple energy balance model for regular building arrays. *Bound-Lay Meteorol* 116:423–443. <https://doi.org/10.1007/s10546-004-7956-x>
25. Kanda M, Moriwaki R, Kasamatsu F (2006) Spatial variability of both turbulent fluxes and temperature profiles in an urban roughness layer. *Bound-Lay Meteorol* 121:339–350. <https://doi.org/10.1007/s10546-006-9063-7>
26. Kays WM, Crawford ME (1993) Convective heat and mass transfer, 3rd edn. McGraw-Hill Inc., New York
27. Klein P, Clark JV (2007) Flow variability in a North American downtown street canyon. *J Appl Meteorol Clim* 46:851–877. <https://doi.org/10.1175/JAM2494.1>
28. Klein PM, Galvez JM (2015) Flow and turbulence characteristics in a suburban street canyon. *Environ Fluid Mech* 15(2):419–438. <https://doi.org/10.1007/s10652-014-9352-5>
29. Krähenbühl ES, Jiang T, Christen A, Martilli A, Oke TR, Bailey BN, Nazarian N, Voogt JA, Giometto MG, Stastny A, Crawford BR (2020) A multi-layer urban canopy meteorological model with trees (BEP-Tree): Street tree impacts on pedestrian-level climate. *Urban Climate* 32:100590. <https://doi.org/10.1016/j.uclim.2020.100590>
30. Lenschow DH, Mann J, Kristensen L (1994) How long is long enough when measuring fluxes and other turbulence statistics? *J Atmos Ocean Tech* 11:661–673
31. Louis JF, Weill A, Vidal-Madjar D (1983) Dissipation length in stable layers. *Bound-Lay Meteorol* 25:229–243. <https://doi.org/10.1007/BF00119538>
32. Louka P, Belcher SE, Harrison RG (2000) Coupling between air flow in streets and the well-developed boundary layer aloft. *Atmos Environ* 34(16):2613–2621. [https://doi.org/10.1016/S1352-2310\(99\)00477-X](https://doi.org/10.1016/S1352-2310(99)00477-X)
33. Martilli A, Clappier A, Rotach MW (2002) An urban surface exchange parameterisation for mesoscale models. *Bound-Lay Meteorol* 104(2):261–304
34. Moradi M, Dyer B, Nazem A, Nambiar MK, Nahian MR, Bueno B, Mackey C, Vasanthakumar S, Nazarian N, Krähenbühl ES, Norford LK, Aliaabadi AA (2021) The vertical city weather generator (VCWG v1.3.2). *Geosci Model Dev* 14(2):961–984. <https://doi.org/10.5194/gmd-14-961-2021>
35. Nambiar MK, Byerlay RAE, Nazem A, Nahian MR, Moradi M, Aliaabadi AA (2020) A Tethered Air Blimp (TAB) for observing the microclimate over a complex terrain. *Geosci Instrum Meth* 9(1):193–211. <https://doi.org/10.5194/gi-9-193-2020>
36. Nelson MA, Pardyjak ER, Brown MJ, Klewicki JC (2007) Properties of the wind field within the Oklahoma City Park Avenue street canyon. Part II: spectra, cospectra, and quadrant analyses. *J Appl Meteorol Clim* 46(12):2055–2073. <https://doi.org/10.1175/2006JAMC1290.1>
37. Nelson MA, Pardyjak ER, Klewicki JC, Pol SU, Brown MJ (2007) Properties of the wind field within the Oklahoma City Park Avenue street canyon. Part I: mean flow and turbulence statistics. *J Appl Meteorol Clim* 46(12):2038–2054. <https://doi.org/10.1175/2006JAMC1427.1>
38. Nelson MA, Pardyjak ER, Klein P (2011) Momentum and turbulent kinetic energy budgets within the Park Avenue street canyon during the Joint Urban 2003 Field Campaign. *Bound-Lay Meteorol* 140(1):143–162. <https://doi.org/10.1007/s10546-011-9610-8>
39. Nieuwstadt FTM (1984) The turbulent structure of the stable, nocturnal boundary layer. *J Atmos Sci* 41(14):2202–2216
40. Offerle B, Eliasson I, Grimmond CSB, Holmer B (2007) Surface heating in relation to air temperature, wind and turbulence in an urban street canyon. *Bound-Lay Meteorol* 122(2):273–292. <https://doi.org/10.1007/s10546-006-9099-8>
41. Ohya Y (2001) Wind-tunnel study of atmospheric stable boundary layers over a rough surface. *Bound-Lay Meteorol* 98(1):57–82. <https://doi.org/10.1023/A:1018767829067>
42. Oke TR (1988) Street design and urban canopy layer climate. *Energ Buildings* 11(1):103–113. [https://doi.org/10.1016/0378-7788\(88\)90026-6](https://doi.org/10.1016/0378-7788(88)90026-6)
43. Oke TR, Mills G, Christen A, Voogt JA (2017) Urban Climates. Cambridge University Press, London. <https://doi.org/10.1017/9781139016476>
44. Patton EG, Sullivan PP, Shaw RH, Finnigan JJ, Weil JC (2016) Atmospheric stability influences on coupled boundary layer and canopy turbulence. *J Atmos Sci* 73(4):1621–1647. <https://doi.org/10.1175/JAS-D-15-0068.1>
45. Pelliccioni A, Monti P, Leuzzi G (2016) Wind-speed profile and roughness sublayer depth modelling in urban boundary layers. *Bound-Lay Meteorol* 160:225–248. <https://doi.org/10.1007/s10546-016-0141-1>
46. Ramamurthy P, Pardyjak ER, Klewicki JC (2007) Observations of the effects of atmospheric stability on turbulence statistics deep within an urban street canyon. *J Appl Meteorol Clim* 46(12):2074–2085. <https://doi.org/10.1175/2007JAMC1296.1>

47. Raupach MR, Thom AS, Edwards I (1980) A wind-tunnel study of turbulent flow close to regularly arrayed rough surfaces. *Bound-Lay Meteorol* 18(4):373–397. <https://doi.org/10.1007/BF00119495>
48. Rotach MW, Vogt R, Bernhofer C, Batchvarova E, Christen A, Clappier A, Feddersen B, Gryning SE, Martucci G, Mayer H, Mitev V, Oke TR, Parlow E, Richner H, Roth M, Roulet YA, Ruffieux D, Salmond JA, Schatzmann M, Voogt JA (2005) BUBBLE—an urban boundary layer meteorology project. *Theor Appl Climatol* 81(3):231–261. <https://doi.org/10.1007/s00704-004-0117-9>
49. Roth M, Inagaki A, Sugawara H, Kanda M (2015) Small-scale spatial variability of turbulence statistics, (co)spectra and turbulent kinetic energy measured over a regular array of cube roughness. *Environ Fluid Mech* 15(2):329–348. <https://doi.org/10.1007/s10652-013-9322-3>
50. Salamanca F, Krayenhoff ES, Martilli A (2009) On the derivation of material thermal properties representative of heterogeneous urban neighborhoods. *J Appl Meteorol Clim* 48(8):1725–1732. <https://doi.org/10.1175/2009JAMC2176.1>
51. Santamouris M, Papanikolaou N, Koronakis I, Livada I, Asimakopoulos D (1999) Thermal and air flow characteristics in a deep pedestrian canyon under hot weather conditions. *Atmos Environ* 33(27):4503–4521. [https://doi.org/10.1016/S1352-2310\(99\)00187-9](https://doi.org/10.1016/S1352-2310(99)00187-9)
52. Schiavon M, Tampieri F, Bosveld FC, Mazzola M, Castelli ST, Viola AP, Yagüe C (2019) The share of the mean turbulent kinetic energy in the near-neutral surface layer for high and low wind speeds. *Bound-Lay Meteorol* 172:81–106. <https://doi.org/10.1007/s10546-019-00435-6>
53. Stull RB (1988) An introduction to boundary layer meteorology. Kluwer Academic Publishers, Dordrecht, The Netherlands. <https://doi.org/10.1007/978-94-009-3027-8>
54. Taylor GI (1938) The spectrum of turbulence. *Proc Roy Soc Lond A* 164:476–490
55. Theeuwes NE, Ronda RJ, Harman IN, Christen A, Grimmond CSB (2019) Parametrizing horizontally-averaged wind and temperature profiles in the urban roughness sublayer. *Bound-Lay Meteorol* 173:321–348. <https://doi.org/10.1007/s10546-019-00472-1>
56. Tomas JM, Pourquie MJBM, Jonker HJJ (2016) Stable stratification effects on flow and pollutant dispersion in boundary layers entering a generic urban environment. *Bound-Lay Meteorol* 159(2):221–239. <https://doi.org/10.1007/s10546-015-0124-7>
57. Trini-Castelli S, Falabino S, Mortarini L, Ferrero E, Richiardone R, Anfossi D (2014) Experimental investigation of surface-layer parameters in low wind-speed conditions in a suburban area. *Q J Roy Meteor Soc* 140(683):2023–2036
58. Zajic D, Fernando HJS, Calhoun R, Princevac M, Brown MJ, Pardyjak ER (2011) Flow and turbulence in an urban canyon. *J Appl Meteorol Clim* 50(1):203–223. <https://doi.org/10.1175/2010JAMC2525.1>
59. Zou J, Liu G, Sun J, Zhang H, Yuan R (2015) The momentum flux-gradient relations derived from field measurements in the urban roughness sublayer in three cities in China. *J Geophys Res-Atmos* 120(20):10797–10809. <https://doi.org/10.1002/2015JD023909>

Publisher's Note Springer Nature remains neutral with regard to jurisdictional claims in published maps and institutional affiliations.

Authors and Affiliations

Amir A. Aliabadi¹  · Mohsen Moradi¹ · Ryan A. E. Byerlay¹

 Amir A. Aliabadi
aliabadi@uoguelph.ca

¹ Atmospheric Innovations Research (AIR) Laboratory, School of Engineering, University of Guelph, Ontario N1G 2W1, Canada